TABLE 4. STEPWISE MULTIVARIATE REGRESSION ANALYSIS SHOWING THE RELATIVE CONTRIBUTION OF EACH VARIABLE TO PREDICT CHANGES IN COMPUTED TOMOGRAPHY PARAMETERS OF EMPHYSEMA

	Coefficient	*P* Value	R^2
Change in LAA% (−960)			
Intercept	1.04		
Exacerbation (for the presence of a history of exacerbation)	0.92	<0.0001	0.41
Change in CT-derived lung volume, ml	0.001	0.001	0.10
Cumulative R^2			0.51
Change in D			
Intercept	−0.02		
Exacerbation (for the presence of a history of exacerbation)	−0.03	<0.0001	0.48
Cumulative R^2			0.48

Definition of abbreviations: CT = computed tomography; LAA%, percentage of low-attenuation area.

Exacerbation (two categories; the presence vs. the absence of a history of exacerbation), change in CT-derived lung volume, and baseline LAA% or D were included as candidate independent variables.

After stepwise variable selection, baseline LAA% was excluded in the model for change in LAA%, and baseline D and change in CT-derived lung volumes were excluded in the model for change in D.

suppressive effects on emphysema progression have not been evaluated in clinical studies. Our study is thus of great importance as it emphasizes the need to assess the progression of emphysematous change in studies of COPD exacerbations.

In the present study, the frequency of exacerbations observed was less than that seen in previous clinical trials. Prospective interventional studies such as the Understanding the Potential Long-term Impact of Tiotropium (UPLIFT) Study (38) and the Toward a Revolution in COPD Health (TORCH) Study (39) showed an incidence of exacerbations ranging from 0.73 to 1.13 per person per year. In our study, the rate of exacerbations in all 60 patients (including those with and without a history of exacerbations) averaged 0.36 per person per year (Table E1). There are several potential explanations for the discrepancy in the rate of exacerbations. First, our study design allowed for the prescription of all respiratory therapies, many of which have been shown to lessen the rate of exacerbations (38, 39). In addition, almost all patients received annual influenza vaccinations and about half also received a pneumococcal vaccination. These vaccinations could reduce the risk of exacerbations (40, 41). Second, during the study, we excluded four patients whose chest X-rays showed lung infiltrate suggesting pneumonia because the influence of pneumonia on CT parameters of emphysema is unknown. We also excluded two patients who died of pneumonia. The frequency of exacerbations has been shown to be associated with the risk of pneumonia (42). Third, the baseline and follow-up examinations were performed at least 4 weeks after resolution of the last exacerbation. We excluded three patients from the follow-up study who could not remain exacerbation-free. Fourth, to investigate changes in CT parameters of emphysema, we excluded five patients whose baseline CT showed bronchiectasis. Bronchiectasis has been reported to cause severe exacerbations and lower bacterial colonization (43), which might increase the exacerbation frequency. These exclusions may not have taken place in previous studies. According to the large Evaluation of COPD Longitudinally to Identify Predictive Surrogate Endpoints (ECLIPSE) cohort, there is one phenotype that is susceptible to exacerbations (44). Our exclusion criteria, including the appearance of pneumonia or existence of bronchiectasis, might have made the portion of these exacerbation-susceptible patients relatively low. However, it should be emphasized that even in patients with such a relatively low incidence of exacerbations, changes in CT parameters of emphysema have been shown to be greater than in those without exacerbations.

Although patients with exacerbations might have experienced more exacerbations in the past than those without exacerbations, baseline LAA% did not differ between the two groups. There are several potential explanations for this finding. In addition to a history of exacerbations, other factors such as disease duration could affect baseline LAA%. Although the ECLIPSE Study showed that patients with a history of frequent exacerbations have been shown to experience exacerbations frequently in the following 3 years (44), the development and progression take a long time, and patients with exacerbations might not always have suffered from frequent exacerbations from disease onset to study entry.

We prospectively recorded changes in respiratory symptoms and health care utilization (HCU) events, using a diary card in the present study. Symptom-defined episodes and HCU events were found in 35 and 32 patients, respectively. When we alternatively defined symptomatic episodes or HCU events as an exacerbation, changes in LAA% or D were still significantly different between patients with and without exacerbations (symptomatic episode: median change in LAA%, 1.60 vs. −0.03%/yr, $P = 0.0001$, respectively, and median change in D, −0.05 vs. −0.01/yr, $P = 0.0001$, respectively; HCU: median change in LAA%, 1.62 vs. 0.13%/yr, $P = 0.0001$, respectively, and median change in D, −0.05 vs. −0.01/yr, $P = 0.0001$, respectively).

Failure to inspire to the same extent at the entry and follow-up scan could skew the lung density (45). We measured total lung volume to estimate the influence of inspiration level, using all CT images of the lung. As shown in Table 3, there were no significant changes in these lung volumes within patients. The degrees of changes were not different between patients with and without exacerbations. In stepwise multivariate regression analysis (Table 4), exacerbations contributed to changes in LAA% ($R^2 = 0.41$) or D ($R^2 = 0.48$) independent of changes in lung volume and baseline CT parameters of emphysema. In addition, it is interesting that in these analyses, changes in CT-derived lung volume contributed to changes in LAA% ($R^2 = 0.10$), but not to changes in D. The change in lung volume did not correlate with the change in D not only in the patients with exacerbations, but also in those without exacerbations (Figure E2). These indicate that changes in D in the longitudinal study could be less influenced by the level of inspiration at CT scanning than changes in LAA%.

This study used one scanner to avoid the effects of inter-scanner errors, and we routinely calibrated the equipment using air and water phantoms as in our previous longitudinal study (26). Moreover, CT numbers were corrected in all images using air densities sampled from the intrathoracic trachea of each subject to eliminate the influence of X-ray tube aging. CT numbers in intrathoracic organs could be influenced by the chest wall. Extracorporeal air density might be used to see differences in CT numbers among different CT scanners. However, we used intrathoracic tracheal air density because

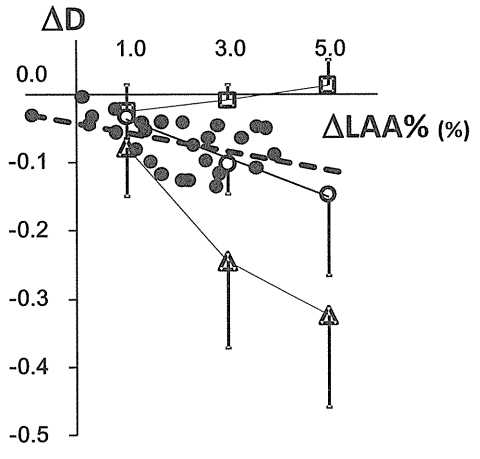

Figure 4. Change in LAA% and D obtained from model simulations and patients with a history of exacerbations. *Open squares* show mean values obtained by model A, which could not allow coalescence of preexisting LAAs. *Open circles* and *open triangles* show mean values obtained by model B15 and B30, respectively, which caused coalescence of LAAs at different rates (15 or 30%). *Error bars* represent the SD. n = 8 per each model. *Solid circles* show original data from patients with a history of exacerbations. The *dotted line* represents the regression line.

the reference should be as close to the target tissue as possible (46) and interscanner variability was not a problem in this study. When we measured LAA% using CT images with a slice thickness of 2 mm in the previous studies (3, 4, 24, 25), the threshold between LAA and normal lung area was defined as −960 Hounsfield units (HU) because the mean −2 standard deviation (SD) of the CT number in the volunteer lungs was approximately −960 HU (47). As a different slice thickness (0.5 mm) might influence the threshold value and data, we calculated LAA% using three threshold values, −910, −930, and −960 HU, to ensure that similar differences of changes in LAA% between patients with and without exacerbations could be detected. When −960 HU was used as the threshold, the baseline LAA% significantly correlated with FEV_1, $\%FEV_1$, and D_{LCO}/V_A. These findings are consistent with our previous reports (3, 4), indicating that −960 HU was a reasonable threshold.

Although baseline FEV_1, $\%FEV_1$, and D_{LCO}/V_A correlated with baseline LAA% and D, changes in LAA% and D did not correlate with changes in FEV_1, $\%FEV_1$, and D_{LCO}/V_A. This might have been because in addition to the extent of emphysema, other factors such as airway remodeling influenced the change in lung function. Moreover, the association of LAA% and D with FEV_1 and D_{LCO}/V_A at study entry was thought to reflect long-term lung inflammatory response and destruction. A 2-year observational period might have been too short to detect correlations of changes in these parameters.

In patients without exacerbations, FEV_1 was significantly decreased after the 2-year follow-up, although LAA% was not changed (Table 3). It should be noted that not only the extent of emphysema or airway remodeling, but also aging itself, might influence the FEV_1 decline. It has been reported in the Framingham Offspring Cohort that FEV_1 decreases by about 20 ml/year even in healthy never-smokers (48).

There are several limitations to the present study. First, the sample size is small. Second, the observational period of 2 years is not long. However, as we performed a single-center study and used only one scanner, the instability of CT scanners was less problematic than in multicenter studies. In addition, exacerbations were prospectively recorded by at least two respiratory physicians who were unaware of CT data. These advantages were thought sufficient to overcome the small sample size and length of observational period. Third, although frequent exacerbations have been reported to be associated with a decline in FEV_1 (5), the present study found no significant difference in annual changes in FEV_1 between the two groups. Additional medications used, such as tiotropium or fluticasone/salmeterol, might make it difficult to detect any differences. Fourth, many exacerbations were treated in the outpatient setting, and few exacerbations required hospitalization (Table E1). We could not assess how the severity of exacerbations would affect the extent of emphysema progression. This should be investigated in future studies. Fifth, because the size of the lung CT voxel could be larger than that of an alveolus and one voxel could not be completely filled with lung tissue, changing from a normal density voxel to a low-attenuation voxel may not strictly correspond to the pathological change of emphysema progression. However, it is well known that LAAs in CT images closely correlate with the extent of pathological emphysema (10–12). We previously demonstrated that D is greatly related to the fractal dimension of the alveolar tissue structure in the lung specimen (4). We thus assume that our methodology can unveil the features of emphysema progression.

In conclusion, emphysema progression assessed by CT was greater in patients with a history of exacerbations than in those without. Both increases in LAA% and decreases in D were found, suggesting that exacerbations are associated with the coalescence of neighboring preexisting LAAs. Hence, the management of exacerbations is important to prevent further emphysema progression.

Author Disclosure: N.T. does not have a financial relationship with a commercial entity that has an interest in the subject of this manuscript. S.M. and T.H. received support from the Grant-in-Aid Program. T.O., K.T., S.M., D.K., and E.O. do not have a financial relationship with a commercial entity that has an interest in the subject of this manuscript. Y.H. and M.M. received support from the Grant-in-Aid Program.

Acknowledgment: The authors thank Akane Haruna, Megumi Kudo, Hirofumi Kiyokawa, and Tamaki Takahashi for assistance with data collection, and Koji Koizumi and Ryuzo Tanaka for technical assistance. The authors also thank Associate Professor Tatsuro Ishizaki and Professor Takeo Nakayama in the Department of Health Informatics at the Kyoto University School of Public Health for help with the statistical analyses.

References

1. Roisin RR. Global strategy for diagnosis, management, and prevention of COPD updated 2009. Available from: http://www.goldcopd.com
2. American Thoracic Society. The definition of emphysema: report of a National Heart, Lung, and Blood Institute, Division of Lung Diseases Workshop. *Am Rev Respir Dis* 1985;132:182–185.
3. Nakano Y, Muro S, Sakai H, Hirai T, Chin K, Tsukino M, Nishimura K, Itoh H, Pare PD, Hogg JC, *et al.* Computed tomographic measurements of airway dimensions and emphysema in smokers: correlation with lung function. *Am J Respir Crit Care Med* 2000;162:1102–1108.
4. Mishima M, Hirai T, Itoh H, Nakano Y, Sakai H, Muro S, Nishimura K, Oku Y, Chin K, Ohi M, *et al.* Complexity of terminal airspace geometry assessed by lung computed tomography in normal subjects and patients with chronic obstructive pulmonary disease. *Proc Natl Acad Sci USA* 1999;96:8829–8834.
5. Donaldson GC, Seemungal TA, Bhowmik A, Wedzicha JA. Relationship between exacerbation frequency and lung function decline in chronic obstructive pulmonary disease. *Thorax* 2002;57:847–852.
6. Seemungal TA, Donaldson GC, Paul EA, Bestall JC, Jeffries DJ, Wedzicha JA. Effect of exacerbation on quality of life in patients with chronic obstructive pulmonary disease. *Am J Respir Crit Care Med* 1998;157:1418–1422.
7. Miravitlles M, Ferrer M, Pont A, Zalacain R, Alvarez-Sala JL, Masa F, Verea H, Murio C, Ros F, Vidal R. Effect of exacerbations on quality of life in patients with chronic obstructive pulmonary disease: a 2 year follow up study. *Thorax* 2004;59:387–395.
8. Soler-Cataluna JJ, Martinez-Garcia MA, Roman Sanchez P, Salcedo E, Navarro M, Ochando R. Severe acute exacerbations and mortality in

patients with chronic obstructive pulmonary disease. *Thorax* 2005;60: 925–931.
9. Wouters EF. The burden of COPD in the Netherlands: results from the Confronting COPD Survey. *Respir Med* 2003;97:S51–S59.
10. Muller NL, Staples CA, Miller RR, Abboud RT. "Density mask": an objective method to quantitate emphysema using computed tomography. *Chest* 1988;94:782–787.
11. Sakai N, Mishima M, Nishimura K, Itoh H, Kuno K. An automated method to assess the distribution of low attenuation areas on chest CT scans in chronic pulmonary emphysema patients. *Chest* 1994;106:1319–1325.
12. Gevenois PA, de Maertelaer V, De Vuyst P, Zanen J, Yernault JC. Comparison of computed density and macroscopic morphometry in pulmonary emphysema. *Am J Respir Crit Care Med* 1995;152:653–657.
13. Madani A, Zanen J, de Maertelaer V, Gevenois PA. Pulmonary emphysema: objective quantification at multi-detector row CT: comparison with macroscopic and microscopic morphometry. *Radiology* 2006;238:1036–1043.
14. Madani A, Van Muylem A, de Maertelaer V, Zanen J, Gevenois PA. Pulmonary emphysema: size distribution of emphysematous spaces on multidetector CT images—comparison with macroscopic and microscopic morphometry. *Radiology* 2008;248:1036–1041.
15. Dirksen A, Piitulainen E, Parr DG, Deng C, Wencker M, Shaker SB, Stockley RA. Exploring the role of CT densitometry: a randomised study of augmentation therapy in α_1-antitrypsin deficiency. *Eur Respir J* 2009;33:1345–1353.
16. Haruna A, Muro S, Nakano Y, Ohara T, Hoshino Y, Ogawa E, Hirai T, Niimi A, Nishimura K, Chin K, *et al.* CT scan findings of emphysema predict mortality in COPD. *Chest* 2010;138:635–640.
17. Mandelbrot B. The fractal geometry of nature. New York: Freeman; 1983.
18. McNamee JE. Fractal perspectives in pulmonary physiology. *J Appl Physiol* 1991;71:1–8.
19. Suki B. Fluctuations and power laws in pulmonary physiology. *Am J Respir Crit Care Med* 2002;166:133–137.
20. Sato A, Hirai T, Imura A, Kita N, Iwano A, Muro S, Nabeshima Y, Suki B, Mishima M. Morphological mechanism of the development of pulmonary emphysema in *klotho* mice. *Proc Natl Acad Sci USA* 2007; 104:2361–2365.
21. Terada K, Muro S, Ohara T, Kudo M, Ogawa E, Hoshino Y, Hirai T, Niimi A, Chin K, Mishima M. Abnormal swallowing reflex and COPD exacerbations. *Chest* 2010;137:326–332.
22. Terada K, Muro S, Ohara T, Haruna A, Marumo S, Kudo M, Ogawa E, Hoshino Y, Hirai T, Niimi A, *et al.* Cough-reflex sensitivity to inhaled capsaicin in COPD associated with increased exacerbation frequency. *Respirology* 2009;14:1151–1155.
23. Terada K, Muro S, Sato S, Ohara T, Haruna A, Marumo S, Kinose D, Ogawa E, Hoshino Y, Niimi A, *et al.* Impact of gastro-oesophageal reflux disease symptoms on COPD exacerbation. *Thorax* 2008;63:951–955.
24. Ogawa E, Nakano Y, Ohara T, Muro S, Hirai T, Sato S, Sakai H, Tsukino M, Kinose D, Nishioka M, *et al.* Body mass index in male patients with COPD: correlation with low attenuation areas on CT. *Thorax* 2009;64:20–25.
25. Ohara T, Hirai T, Muro S, Haruna A, Terada K, Kinose D, Marumo S, Ogawa E, Hoshino Y, Niimi A, *et al.* Relationship between pulmonary emphysema and osteoporosis assessed by CT in patients with COPD. *Chest* 2008;134:1244–1249.
26. Ohara T, Hirai T, Sato S, Terada K, Kinose D, Haruna A, Marumo S, Nishioka M, Ogawa E, Nakano Y, *et al.* Longitudinal study of airway dimensions in chronic obstructive pulmonary disease using computed tomography. *Respirology* 2008;13:372–378.
27. Papi A, Bellettato CM, Braccioni F, Romagnoli M, Casolari P, Caramori G, Fabbri LM, Johnston SL. Infections and airway inflammation in chronic obstructive pulmonary disease severe exacerbations. *Am J Respir Crit Care Med* 2006;173:1114–1121.
28. Mercer PF, Shute JK, Bhowmik A, Donaldson GC, Wedzicha JA, Warner JA. MMP-9, TIMP-1 and inflammatory cells in sputum from COPD patients during exacerbation. *Respir Res* 2005;6:151.
29. Drost EM, Skwarski KM, Sauleda J, Soler N, Roca J, Agusti A, MacNee W. Oxidative stress and airway inflammation in severe exacerbations of COPD. *Thorax* 2005;60:293–300.
30. Qiu Y, Zhu J, Bandi V, Atmar RL, Hattotuwa K, Guntupalli KK, Jeffery PK. Biopsy neutrophilia, neutrophil chemokine and receptor gene expression in severe exacerbations of chronic obstructive pulmonary disease. *Am J Respir Crit Care Med* 2003;168: 968–975.
31. Mitsunobu F, Ashida K, Hosaki Y, Tsugeno H, Okamoto M, Nishida K, Takata S, Yokoi T, Mishima M, Tanizaki Y. Complexity of terminal airspace geometry assessed by computed tomography in asthma. *Am J Respir Crit Care Med* 2003;167:411–417.
32. Coxson HO, Whittall KP, Nakano Y, Rogers RM, Sciurba FC, Keenan RJ, Hogg JC. Selection of patients for lung volume reduction surgery using a power law analysis of the computed tomographic scan. *Thorax* 2003;58:510–514.
33. Martinez FJ, Foster G, Curtis JL, Criner G, Weinmann G, Fishman A, DeCamp MM, Benditt J, Sciurba F, Make B, *et al.* Predictors of mortality in patients with emphysema and severe airflow obstruction. *Am J Respir Crit Care Med* 2006;173:1326–1334.
34. Davies L, Angus RM, Calverley PM. Oral corticosteroids in patients admitted to hospital with exacerbations of chronic obstructive pulmonary disease: a prospective randomised controlled trial. *Lancet* 1999; 354:456–460.
35. Thompson WH, Nielson CP, Carvalho P, Charan NB, Crowley JJ. Controlled trial of oral prednisone in outpatients with acute COPD exacerbation. *Am J Respir Crit Care Med* 1996;154:407–412.
36. Niewoehner DE, Erbland ML, Deupree RH, Collins D, Gross NJ, Light RW, Anderson P, Morgan NA; Department of Veterans Affairs Cooperative Study Group. Effect of systemic glucocorticoids on exacerbations of chronic obstructive pulmonary disease. *N Engl J Med* 1999;340:1941–1947.
37. Stockley RA, O'Brien C, Pye A, Hill SL. Relationship of sputum color to nature and outpatient management of acute exacerbations of COPD. *Chest* 2000;117:1638–1645.
38. Tashkin DP, Celli B, Senn S, Burkhart D, Kesten S, Menjoge S, Decramer M. A 4-year trial of tiotropium in chronic obstructive pulmonary disease. *N Engl J Med* 2008;359:1543–1554.
39. Calverley PM, Anderson JA, Celli B, Ferguson GT, Jenkins C, Jones PW, Yates JC, Vestbo J. Salmeterol and fluticasone propionate and survival in chronic obstructive pulmonary disease. *N Engl J Med* 2007; 356:775–789.
40. Wongsurakiat P, Maranetra KN, Wasi C, Kositanont U, Dejsomritrutai W, Charoenratanakul S. Acute respiratory illness in patients with COPD and the effectiveness of influenza vaccination: a randomized controlled study. *Chest* 2004;125:2011–2020.
41. Alfageme I, Vazquez R, Reyes N, Munoz J, Fernandez A, Hernandez M, Merino M, Perez J, Lima J. Clinical efficacy of anti-pneumococcal vaccination in patients with COPD. *Thorax* 2006;61:189–195.
42. Crim C, Calverley PM, Anderson JA, Celli B, Ferguson GT, Jenkins C, Jones PW, Willits LR, Yates JC, Vestbo J. Pneumonia risk in COPD patients receiving inhaled corticosteroids alone or in combination: TORCH Study results. *Eur Respir J* 2009;34:641–647.
43. Patel IS, Vlahos I, Wilkinson TM, Lloyd-Owen SJ, Donaldson GC, Wilks M, Reznek RH, Wedzicha JA. Bronchiectasis, exacerbation indices, and inflammation in chronic obstructive pulmonary disease. *Am J Respir Crit Care Med* 2004;170:400–407.
44. Hurst JR, Vestbo J, Anzueto A, Locantore N, Mullerova H, Tal-Singer R, Miller B, Lomas DA, Agusti A, Macnee W, *et al.* Susceptibility to exacerbation in chronic obstructive pulmonary disease. *N Engl J Med* 2010;363:1128–1138.
45. Coxson HO, Mayo J, Lam S, Santyr G, Parraga G, Sin DD. New and current clinical imaging techniques to study chronic obstructive pulmonary disease. *Am J Respir Crit Care Med* 2009;180:588–597.
46. Boden SD, Goodenough DJ, Stockham CD, Jacobs E, Dina T, Allman RM. Precise measurement of vertebral bone density using computed tomography without the use of an external reference phantom. *J Digit Imaging* 1989;2:31–38.
47. Mishima M, Hirai T, Jin Z, Oku Y, Sakai N, Nakano Y, Sakai H, Chin K, Ohi M, Kawakami K, *et al.* Standardization of low attenuation area versus total lung area in chest X-ray CT as an indicator of chronic pulmonary emphysema. *Front Med Biol Eng* 1997;8:79–86.
48. Kohansal R, Martinez-Camblor P, Agusti A, Buist AS, Mannino DM, Soriano JB. The natural history of chronic airflow obstruction revisited: an analysis of the Framingham Offspring Cohort. *Am J Respir Crit Care Med* 2009;180:3–10.

nature medicine

Prostaglandin $F_{2\alpha}$ receptor signaling facilitates bleomycin-induced pulmonary fibrosis independently of transforming growth factor-β

Toru Oga[1,2], Toshiyuki Matsuoka[1], Chengcan Yao[1], Kimiko Nonomura[1], Shiho Kitaoka[1], Daiji Sakata[1], Yoshihiro Kita[3], Kiminobu Tanizawa[4], Yoshio Taguchi[5], Kazuo Chin[2], Michiaki Mishima[4], Takao Shimizu[3] & Shuh Narumiya[1]

Idiopathic pulmonary fibrosis (IPF) is a progressive disease characterized by fibroblast proliferation and excess deposition of collagen and other extracellular matrix (ECM) proteins, which lead to distorted lung architecture and function[1]. Given that anti-inflammatory or immunosuppressive therapy currently used for IPF does not improve disease progression therapies targeted to blocking the mechanisms of fibrogenesis are needed[1]. Although transforming growth factor-β (TGF-β) functions are crucial in fibrosis[2,3], antagonizing this pathway in bleomycin-induced pulmonary fibrosis, an animal model of IPF, does not prevent fibrosis completely[4–7], indicating an additional pathway also has a key role in fibrogenesis. Given that the loss of cytosolic phospholipase A_2 ($cPLA_2$) suppresses bleomycin-induced pulmonary fibrosis[8], we examined the roles of prostaglandins using mice lacking each prostoaglandin receptor[9–15]. Here we show that loss of prostaglandin F (PGF) receptor (FP) selectively attenuates pulmonary fibrosis while maintaining similar levels of alveolar inflammation and TGF-β stimulation as compared to wild-type (WT) mice, and that FP deficiency and inhibition of TGF-β signaling additively decrease fibrosis. Furthermore, $PGF_{2\alpha}$ is abundant in bronchoalveolar lavage fluid (BALF) of subjects with IPF and stimulates proliferation and collagen production of lung fibroblasts via FP, independently of TGF-β. These findings show that $PGF_{2\alpha}$-FP signaling facilitates pulmonary fibrosis independently of TGF-β and suggests this signaling pathway as a therapeutic target for IPF.

$cPLA_2$ cleaves phospholipids in response to stimuli and releases arachidonic acid, which is metabolized by cyclooxygenase (COX) to produce prostaglandins and by 5-lipoxygenase to produce leukotrienes. Prostaglandins, including PGD_2, PGE_2, $PGF_{2\alpha}$, PGI_2 and thromboxane A_2 (TXA_2), act at their cognate receptors designated as DP (*Ptgdr*), EP1–EP4 (*Ptger1–Ptger4*), FP (*Ptgfr*), IP (*Ptgir*) and TP (*Ptgtr*), respectively[16]. We examined the action of each prostaglandin receptor in pulmonary fibrosis by subjecting *Ptgdr*$^{-/-}$, *Ptger1*$^{-/-}$, *Ptger2*$^{-/-}$, *Ptger3*$^{-/-}$, *Ptgfr*$^{-/-}$, *Ptgir*$^{-/-}$ and *Ptgtr*$^{-/-}$ mice in the C57BL/6 background to bleomycin-induced pulmonary fibrosis[3,8]. Because *Ptger4*$^{-/-}$ mice die neonatally in the C57BL/6 background[11], we instead administered a selective EP4 antagonist, ONO-AE3-208, at 10 mg per kg body weight per day to WT mice to examine EP4 action[17]. We administered bleomycin to the mice in the trachea and killed them on day 21 after treatment when fibrosis reached its peak (**Supplementary Fig. 1a**). We evaluated fibrosis biochemically by measuring the hydroxyproline content, a marker for collagen, in the lung and histologically by Masson's trichrome staining. Among the seven lines of genetic knockout mice and the one group of mice treated with an antagonist, only *Ptgfr*$^{-/-}$ mice showed significantly less hydroxyproline content than WT control mice ($P = 0.018$) (**Fig. 1a** and **Supplementary Fig. 1b**). Impaired collagen deposition in *Ptgfr*$^{-/-}$ mice was confirmed histologically in lung sections (**Fig. 1b**). Whereas bleomycin treatment in WT mice led to alveolar thickening caused by marked cell accumulation and intense matrix protein deposition, *Ptgfr*$^{-/-}$ mice showed less matrix protein deposition and less cellularity than WT mice (**Fig. 1b**). We prepared lung cell suspensions and determined the number of fibroblasts and macrophages by flow cytometry, as measured by the number of type I collagen (Col I)$^+$ and CD11b$^+$ cells, respectively. *Ptgfr*$^{-/-}$ mice had significantly fewer Col I$^+$ cells than WT mice ($P = 0.016$), but the number of CD11b$^+$ cells was not significantly different (**Supplementary Table 1**). We then examined the lung functions of these mice with the Flexivent system[8]. Lung elastance, a marker for lung stiffness, which was of the same level in saline-treated WT and *Ptgfr*$^{-/-}$ mice, was significantly higher in WT mice with the bleomycin treatment ($P = 0.0035$) but not in the bleomycin-treated *Ptgfr*$^{-/-}$ mice ($P = 0.75$) (**Fig. 1c**). Thus, the loss of FP resulted in a substantial reduction of fibrotic response and spared lung function.

We next examined inflammatory responses in *Ptgfr*$^{-/-}$ mice by examining the number and composition of cells recovered in BALF. The inflammatory responses examined by this procedure peaked on day 7 after bleomycin administration (**Supplementary Fig. 2a**).

[1]Department of Pharmacology, [2]Department of Respiratory Care and Sleep Control Medicine, Kyoto University Faculty of Medicine, Kyoto, Japan. [3]Department of Biochemistry and Molecular Biology, University of Tokyo Faculty of Medicine, Tokyo, Japan. [4]Department of Respiratory Medicine, Kyoto University Faculty of Medicine, Kyoto, Japan. [5]Department of Respiratory Medicine, Tenri Hospital, Nara, Japan. Correspondence should be addressed to S.N. (snaru@mfour.med.kyoto-u.ac.jp).

Received 14 September; accepted 31 October; published online 29 November 2009; doi:10.1038/nm.2066

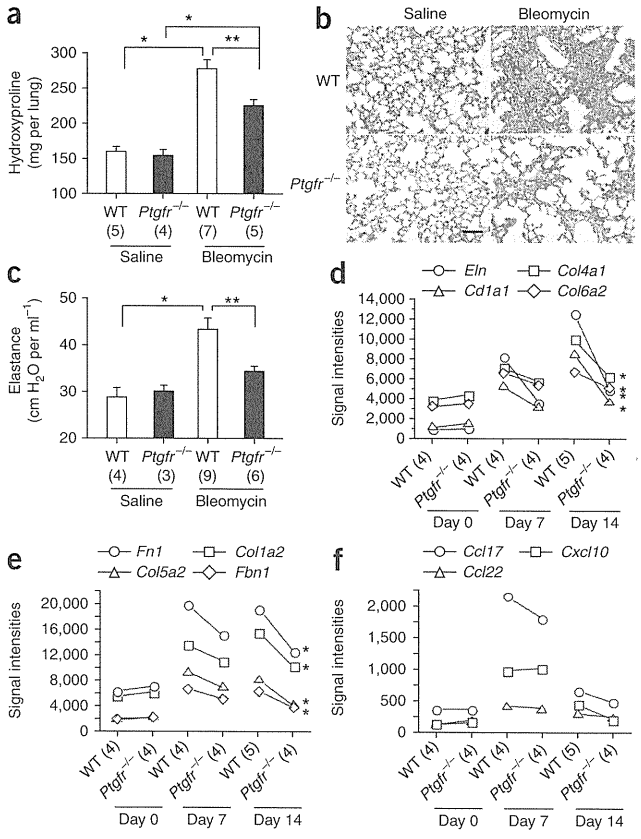

Figure 1 Bleomycin-induced pulmonary fibrosis in *Ptgfr*$^{-/-}$ mice. (**a**) Hydroxyproline contents of the lung from WT and *Ptgfr*$^{-/-}$ mice on day 21 after saline or bleomycin treatment. $*P < 0.01$ versus each saline-treated group. $**P < 0.05$ versus the bleomycin-treated WT group. (**b**) Typical photomicrographs of Masson's trichrome staining of the lung from WT or *Ptgfr*$^{-/-}$ mice on day 21 after saline or bleomycin treatment. Scale bar, 100 μm. (**c**) Lung elastance of WT and *Ptgfr*$^{-/-}$ mice examined with the Flexivent system on day 21 after saline or bleomycin treatment. $*P < 0.01$ versus the saline-treated WT group. $**P < 0.05$ versus the bleomycin-treated WT group. (**d–f**) Microarray analysis of gene expression of WT and *Ptgfr*$^{-/-}$ lungs on days 0, 7 and 14 after bleomycin treatment (see also **Supplementary Fig. 3a,b** and **Supplementary Table 3**). Changes in signal intensity of representative genes in cluster 13 (**d**), cluster 15 (**e**) and cluster 14 (**f**) in WT and *Ptgfr*$^{-/-}$ mice are shown. *Eln* encodes elastin; *Fn1* encodes fibronectin-1; *Fbn1* encodes fibrillin-1. $*P < 0.05$ versus the WT group. Numbers in parentheses in **a**, **c** and **d–f** indicate the number of mice of each group. Error bars represent s.e.m.

We found no difference in either the number or the composition of BALF cells between WT and *Ptgfr*$^{-/-}$ mice on days 0, 3, 7 and 21 after bleomycin treatment (**Supplementary Fig. 2a–e**). There was also no difference in the T and B cell subsets of lymphocytes on day 7 (**Supplementary Table 2**).

The above results suggest that the lack of FP attenuates fibrosis without change in inflammation. To therefore pinpoint the actual role of FP action in the development of fibrosis, we performed gene expression analysis in the lungs of WT and *Ptgfr*$^{-/-}$ mice on days 0, 7 and 14 after bleomycin treatment. We extracted and analyzed 2,217 fluctuating genes, which we divided into 15 clusters on the basis of their induction pattern (**Supplementary Fig. 3a,b**). We found that clusters 13 and 15 contained fibrosis-related genes, and there was a marked difference in the pattern or extent of their induction between WT and *Ptgfr*$^{-/-}$ mice (**Fig. 1d,e** and **Supplementary Table 3**). For example, cluster 13, composed of 271 genes, contains genes encoding several isoforms of collagen (*Col4a1*, *Col1a1* and *Col6a2*) and elastin, which were induced on day 7 and continued to increase until day 14 in WT mice (**Fig. 1d** and **Supplementary Table 3**). However, these genes were induced to a lesser extent on days 7 and 14 in *Ptgfr*$^{-/-}$ mice (**Fig. 1d** and **Supplementary Table 3**). Similarly, cluster 15 (478 genes) contains genes encoding other isoforms of collagen (*Col1a2* and *Col5a2*), fibronectin-1, tenascin C, fibrillin-1 and thrombospondin-1. These genes were induced on day 7 and remained unchanged until day 14 in WT mice, whereas their expression increased to a lesser degree on days 7 and 14 in *Ptgfr*$^{-/-}$ mice (**Fig. 1e** and **Supplementary Table 3**). Cluster 15 also contains genes involved in the regulation of fibrosis, such as those encoding insulin-like growth factor-1, plasminogen activator inhibitor-1 and connective tissue growth factor. Expression of these genes was also suppressed at either day 7 or day 14 in *Ptgfr*$^{-/-}$ mice compared to WT mice (**Supplementary Table 3**). In contrast, cluster 14 (275 genes) contained genes encoding chemokines such as CCL17, CCL22 and CXCL10. Expression of these inflammation-related genes increased on day 7 and decreased on day 14 similarly in WT and *Ptgfr*$^{-/-}$ mice (**Fig. 1f** and **Supplementary Table 3**). These findings thus suggest that $PGF_{2\alpha}$-FP signaling functions not in inflammation but in fibrosis, where it facilitates fibrogenesis by enhancing expression of fibrosis-related genes.

TGF-β is typically secreted as an inactive latent enzyme, and it is extracellular activation that drives fibrosis. Excessive and sustained production of active TGF-β is therefore regarded as a key event in tissue fibrosis[2,3]. To dissect the effects of $PGF_{2\alpha}$-FP signaling on the TGF-β pathway, we first measured the content of active TGF-β1 in BALF obtained from WT and *Ptgfr*$^{-/-}$ mice after bleomycin treatment. The amount of active TGF-β1 increased from day 0 to day 7 and remained high on day 21 and showed no difference between WT and *Ptgfr*$^{-/-}$ mice on either day (**Fig. 2a**). We next examined phosphorylation of Smad2, a downstream signaling molecule of TGF-β, the phosphorylation of which is regarded as the crucial intracellular step in TGF-β signal transduction[6], in the lung homogenate prepared from WT and *Ptgfr*$^{-/-}$ mice on days 0 and 7. We observed a comparable increase in Smad2 phosphorylation after bleomycin treatment in the two genotypes of mice (**Fig. 2b**). Additionally, microarray data showed a similar decrease in *Smad7* expression, an endogenous inhibitor of Smad signaling in response to TGF-β activation, in WT and *Ptgfr*$^{-/-}$ mice (data not shown). These results negate a role of FP in regulating endogenous TGF-β production and in TGF-β–Smad signaling. To verify further that FP functions independently of TGF-β signaling in pulmonary fibrosis, we administered a TGF-β receptor I kinase inhibitor, SD-208 (ref. 7), to WT and *Ptgfr*$^{-/-}$ mice. Both the genetic loss of FP and the SD-208 administration suppressed the increase in the hydroxyproline content in the lung, and, when combined, caused an additive suppression (**Fig. 2c**), indicating that the TGF-β pathway and $PGF_2\alpha$-FP signaling work independently of each other in the development of lung fibrosis.

The above results suggest a possibility that FP is directly involved in fibrogenesis in the lung. Consistently, quantitative RT-PCR analysis detected *Ptgfr* expression in the whole lung as well as in isolated lung fibroblasts (**Fig. 2d**). These results suggested that fibroblasts, key mediators in fibrogenesis, mediate FP action, although they did not exclude an additional contribution by other cell types. The apparent decrease in the *Ptgfr* expression in the whole lung in spite of the increased number of fibroblasts at day 7 may be due to a relative abundance of infiltrating inflammatory cells at this time. *Ptgfr* expression in

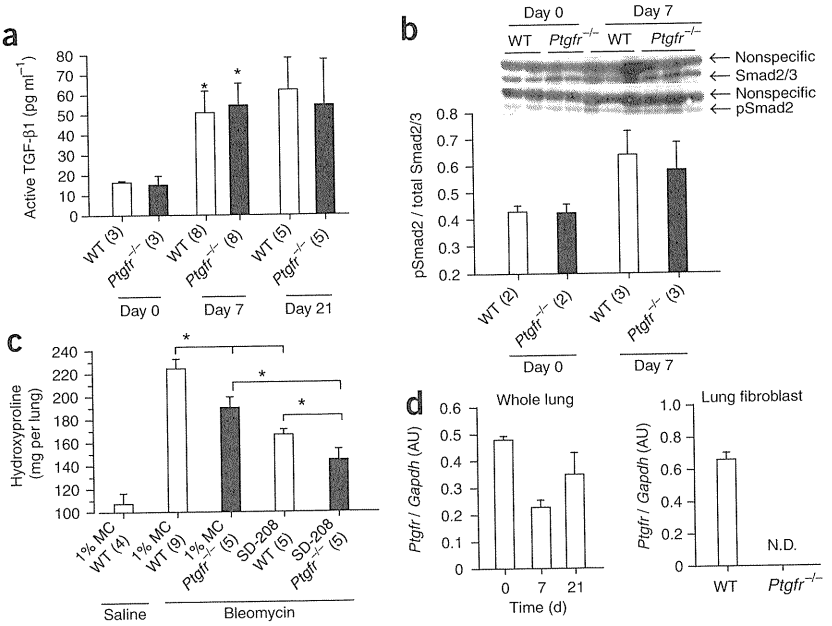

Figure 2 TGF-β1–independent action of FP signaling in pulmonary fibrosis. (**a**) Amounts of active TGF-β1 in BALF of WT and *Ptgfr*$^{-/-}$ mice on days 0, 7 and 21 after bleomycin treatment. *$P < 0.05$ versus each group on day 0. (**b**) Western blot analysis of Smad2 phosphorylation in lung homogenates from WT and *Ptgfr*$^{-/-}$ mice on days 0 and 7 after bleomycin treatment. A typical immunoblot (top) and a ratio of the density of pSmad2 to that of Smad2/3 analyzed with densitometry (bottom) are shown. (**c**) Hydroxyproline contents of the lung from WT and *Ptgfr*$^{-/-}$ mice on day 21 after saline or bleomycin treatment with or without SD-208 administration. MC, methylcellulose used as a vehicle. *$P < 0.05$ for indicated comparison. Numbers in parentheses in **a**–**c** indicate the number of mice of each group. (**d**) Real-time RT-PCR for *Ptgfr* expression in whole lung ($n = 2$ or 3) (left) on days 0, 7 and 21 after bleomycin instillation and in WT and *Ptgfr*$^{-/-}$ lung fibroblasts ($n = 3$) (right). *Ptgfr* expression is normalized to that of *Gapdh*. ND, not detected. Error bars represent s.e.m.

fibroblasts in the lung was further indicated histologically by staining for β-galactosidase knocked into the *Ptgfr* locus in *Ptgfr*$^{-/-}$ mice[13] (**Supplementary Fig. 4**).

We next used liquid chromatography–tandem mass spectrometry[18,19] to systematically analyze the amount of arachidonic acid metabolites in the lung. We first used mice subjected to the bleomycin model. $PGF_{2\alpha}$ was present in substantial amounts in the lungs of mice during pulmonary fibrosis and reached its peak on day 14 after treatment (**Supplementary Table 4**). In this model, PGE_2, its metabolite 13,14-dihydro-15-keto-PGE_2 and 6-keto-$PGF_{1\alpha}$ (a stable metabolite of PGI_2) were by far the most abundant products, which may reflect the inflammatory process in this model (**Supplementary Table 4**). We next analyzed the metabolites in BALF from subjects with IPF or sarcoidosis. The concentrations of $PGF_{2\alpha}$ and PGE_2 were high in the subjects with IPF compared to those in the subjects with sarcoidosis ($P = 0.071$ for $PGF_{2\alpha}$), whereas PGD_2 and TXA_2 concentrations were at the same level in the two groups of subjects (**Table 1**). $PGF_{2\alpha}$ and other COX metabolites were more abundant than leukotrienes in BALF of these subjects (**Table 1**).

Finally, we examined the effects of FP stimulation on proliferation and collagen production of lung fibroblasts. $PGF_{2\alpha}$ stimulated proliferation of mouse lung fibroblasts at concentrations starting at 30 nM, additively to platelet-derived growth factor-BB (PDGF-BB), a well-known stimulator of lung fibroblasts[20], and this stimulatory effect was absent in *Ptgfr*$^{-/-}$ fibroblasts (**Fig. 3a**). TGF-β had a marginal effect under our experimental conditions (data not shown). In contrast, $PGF_{2\alpha}$ significantly increased collagen production in WT fibroblasts in a manner additive to stimulation with TGF-β1 (**Fig. 3b**). This effect was absent in fibroblasts from *Ptgfr*$^{-/-}$ mice, whereas TGF-β1 increased collagen production in *Ptgfr*$^{-/-}$ fibroblasts (**Fig. 3b**). These results indicate that $PGF_{2\alpha}$ can stimulate both proliferation and collagen production of mouse lung fibroblasts via FP independently of TGF-β.

We then confirmed the TGF-β–independent, FP-mediated collagen production in human lung fibroblasts. We used IMR90, a human lung fibroblast cell line, which expressed *PTGFR*, as examined by RT-PCR (**Fig. 3c**). Consistent with the findings in mouse lung fibroblasts, $PGF_{2\alpha}$ and PDGF-BB significantly stimulated proliferation of IMR90 cells (**Fig. 3d**), and both TGF-β1 and $PGF_{2\alpha}$ increased collagen production in IMR90 cells in a dose-dependent fashion (**Supplementary Fig. 5a,b**). The effect of TGF-β1 on collagen production was inhibited by a TGF receptor type I kinase inhibitor, SB-505124 (ref. 21), but not by a selective FP receptor antagonist, AL8810 (ref. 22) (**Fig. 3e,f**). Conversely, the effect of $PGF_{2\alpha}$ was inhibited by AL8810 but not by SB-505124 (**Fig. 3e,f**). Furthermore, $PGF_{2\alpha}$ and TGF-β1 induced collagen production additively in IMR90 cells (**Fig. 3g**). These results corroborated our evidence that $PGF_{2\alpha}$ and TGF-β1 induce collagen production independently.

Table 1 Arachidonic acid metabolites in BALF of subjects with lung diseases

	IPF	Sarcoidosis
Number of subjects, (male/female)	13/2	7/5
Age (years)	69 ± 1	41 ± 4
PGD_2 (pg ml^{-1})	26 ± 8	28 ± 14
PGE_2 (pg ml^{-1})	19 ± 5	10 ± 3
$PGF_{2\alpha}$ (pg ml^{-1})	20 ± 6	8 ± 1
6-keto-$PGF_{1\alpha}$ (pg ml^{-1})	14 ± 5	9 ± 6
TXB_2 (pg ml^{-1})	8 ± 1	8 ± 3
LTB_4 (pg ml^{-1})	8 ± 5	1 ± 1
LTC_4 (pg ml^{-1})	1 ± 0	1 ± 0
LTD_4 (pg ml^{-1})	0 ± 0	1 ± 0
5-HETE (pg ml^{-1})	8 ± 2	4 ± 1
8-HETE (pg ml^{-1})	3 ± 1	2 ± 0
11-HETE (pg ml^{-1})	3 ± 0	2 ± 0
12-HETE (pg ml^{-1})	36 ± 7	28 ± 5
15-HETE (pg ml^{-1})	133 ± 22	109 ± 20
13,14-dihydro-15keto-PGD_2 (pg ml^{-1})	0 ± 0	1 ± 1
13,14-dihydro-15keto-PGE_2 (pg ml^{-1})	15 ± 9	5 ± 3
13,14-dihydro-15keto-$PGF_{2\alpha}$ (pg ml^{-1})	7 ± 3	4 ± 2
PGJ_2 + 12-deoxy-PGJ_2 (pg ml^{-1})	1 ± 0	1 ± 0
15-deoxy-PGJ_2 (pg ml^{-1})	6 ± 2	6 ± 1
12-HHT (pg ml^{-1})	19 ± 7	40 ± 9

Results are presented as means ± s.e.m. HETE, hydroxyeicosatetraenoic acid; 12-HHT, 12-hydroxy-5,8,10-heptadecatrienoic acid.

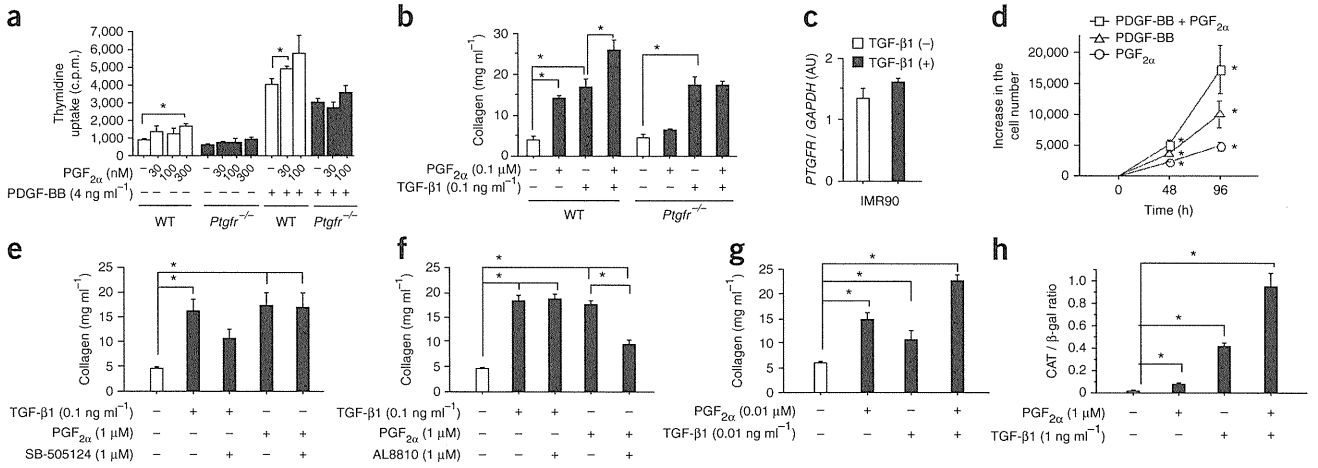

Figure 3 Effects of $PGF_{2\alpha}$ on proliferation and collagen production of lung fibroblasts. (**a**) [^{3}H]thymidine incorporation of WT and *Ptgfr*$^{-/-}$ lung fibroblasts incubated with the indicated concentrations of $PGF_{2\alpha}$ in the presence or absence of PDGF-BB ($n = 3$ each). (**b**) Collagen production of WT and *Ptgfr*$^{-/-}$ lung fibroblasts incubated with the indicated concentrations of $PGF_{2\alpha}$ and TGF-β1 ($n = 3$). The amounts of secreted soluble collagen are shown. (**c**) Real-time RT-PCR for *PTGFR* expression in IMR90 cells in the presence or absence of TGF-β1 ($n = 3$). *PTGFR* expression is normalized to that of *GAPDH*. (**d**) Proliferation of IMR90 cells in the presence of 0.1 μM $PGF_{2\alpha}$ or 20 ng ml^{-1} PDGF-BB or both in DMEM containing 0.5% FBS. The increase in cell number with each treatment is shown. $^*P < 0.05$ versus control culture without any addition. (**e**,**f**) Collagen production of IMR90 cells stimulated with TGF-β1 or $PGF_{2\alpha}$ in the presence or absence of SB-505124 ($n = 3$–6) (**e**) or AL8810 ($n = 3$–4) (**f**). The amount of secreted soluble collagen is shown. (**g**) Collagen production of IMR90 cells incubated with $PGF_{2\alpha}$ alone, TGF-β1 alone or both ($n = 3$). (**h**) Promoter activity of the −3500*COL1A2/CAT* reporter in IMR90 cells stimulated with the indicated concentrations of $PGF_{2\alpha}$ or TGF-β1 or both ($n = 4$ or 5). The *COL1A2* promoter activity, measured as the CAT amount, is normalized to expression of *lacz* transfected together with the reporter plasmid, and is shown as the CAT/β-galactosidase ratio. $^*P < 0.05$ for indicated comparison in **a**,**b** and **e**–**h**. Error bars represent s.e.m.

We observed enhanced collagen production by $PGF_{2\alpha}$ and TGF-β1 also in LL29 cells (the human IPF lung fibroblast cell line) and WI38 cells (the human normal lung fibroblast cell line) (**Supplementary Fig. 5c,d**).

To examine the mechanism by which $PGF_{2\alpha}$ and TGF-β1 induce collagen production, we transfected IMR90 cells with the −3500*COL1A2/CAT* reporter construct (described in the **Supplementary Methods**)[23,24] and examined the effects of $PGF_{2\alpha}$ or TGF-β1 on the promoter activity. Both $PGF_{2\alpha}$ and TGF-β1 increased the promoter activity of *COL1A2*, and simultaneous addition of $PGF_{2\alpha}$ and TGF-β1 synergistically increased the CAT induction (**Fig. 3h**). These results suggest that FP stimulation functions at the transcriptional level to induce collagen production. Consistently, $PGF_{2\alpha}$ increased *COL1A2* expression in a dose-dependent fashion (**Supplementary Fig. 5e**). We further showed the involvement of $PGF_{2\alpha}$ in bleomycin-induced fibrosis by treating IMR90 cells expressing the *COL1A2* promoter with lung homogenates from the bleomycin-challenged mice in the absence or presence of AL8810. The addition of the homogenate increased *COL1A2* expression, which was reduced by 37% by treatment with AL8810 (**Supplementary Fig. 5f**). We further examined the downstream signaling of FP by examining the effects of various kinase inhibitors on $PGF_{2\alpha}$-induced collagen production. Among the inhibitors, Y-27632 (ref. 25), a specific Rho-associated coiled-coil–containing kinase (also called Rho kinase) inhibitor, inhibited $PGF_{2\alpha}$-induced collagen production in IMR90 cells in a concentration-dependent manner (**Supplementary Fig. 5g,h**). This inhibitor, however, did not inhibit the TGF-β1–induced collagen production (**Supplementary Fig. 5i**). In contrast, a specific inhibitor of Smad3, SIS3 (ref. 26), inhibited the TGF-β1–induced collagen production but not that inducded by $PGF_{2\alpha}$ (**Supplementary Fig. 5i**), suggesting that TGF-β1 and $PGF_{2\alpha}$ mobilize different signaling to induce collagen production.

Here we used bleomycin-induced pulmonary fibrosis, a mouse model of IPF, and found that $PGF_{2\alpha}$-FP signaling mediates pulmonary fibrosis additive to that induced by TGF-β. IPF is a disease without effective treatment that affects seven to ten people per 100,000 per year, with a median survival of 3–5 years[27]. Efforts have been focused on developing drugs targeted to molecular events in fibrosis[1,28], and, currently, therapy against TGF-β seems to be the most promising candidate. However, whether therapy against TGF-β therapy can be an optimal treatment for IPF is under debate, given the diverse functions of this cytokine in various diseases[2,29,30]. The unique profile of $PGF_{2\alpha}$-FP signaling described above suggests that inhibition of this signaling pathway may be a potential and alternative approach to ameliorate pulmonary fibrosis.

Indeed, we detected $PGF_{2\alpha}$ as a major COX metabolite together with PGD_2, PGE_2 and 6-keto-$PGF_{1\alpha}$, a degradation metabolite of PGI_2, in the BALF of subjects with IPF. PGE_2 and PGD_2 may cross-react on FP to induce profibrotic actions, given their abundance in the lung and their binding affinity to FP[16]. In contrast, PGE_2 and PGI_2 were previously indicated to function protectively against bleomycin-induced pulmonary fibrosis through EP2 (ref. 31) and IP (ref. 32). Although we did not reproduce such phenotypes, this may be a result of the differences in the bleomycin dose used[32] or the methods used for collagen measurements, the Sircol dye–binding method[31] versus hydroxyproline measurement. Among leukotrienes, LTB_4 or LTC_4 was detected in the lungs of bleomycin-treated mice or the BALF of subjects with IPF. LTC_4 may exert proinflammatory action, and it contributes to fibrosis, as indicated by studies on mice deficient in 5-lipoxygenase[33] or cysteinyl LT_2 receptor[34]. Thus, the various arachidonate metabolites seem to have various roles in pulmonary fibrosis and modify the disease process. $cPLA_2$ cleaves phospholipids and yields lysophospholipids along with arachidonic acid. A recent study reported that lysophosphatidic acid acts on lysophosphatidic acid receptor-1 to induce fibroblast recruitment and contributes to pulmonary fibrosis[35]. Thus, $PGF_{2\alpha}$ and lysophosphatidic acid, the two products derived from breakdown of phospholipids by $cPLA_2$,

contribute complementarily to fibrosis. $PGF_{2\alpha}$ is one of the classic prostaglandins. Yet, elucidation of its physiological functions has been somehow neglected, except for its function as a key regulator of parturition and the use of an FP agonist as an antiglaucoma agent[13,16]. Our study has shed light on this neglected prostaglandin as a regulator of pulmonary fibrosis. This knowledge may be exploited to develop a new category of antifibrotic drugs to treat IPF.

METHODS

Methods and any associated references are available in the online version of the paper at http://www.nature.com/naturemedicine/.

Accession codes. Microarray data have been deposited in Gene Expression Omnibus with accession code GSE18800.

Note: Supplementary information is available on the Nature Medicine website.

ACKNOWLEDGMENTS

We thank M. Trojanowska (Medical University of South Carolina) and H. Ihn (Kumamoto University) for the –3500*COL1A2/CAT* construct, and Ono Pharmaceutical Company for ONO-AE3-208. We also thank Y. Kobashi for BALF analysis, T. Fujiwara for animal care and T. Arai for assistance. This work was supported in part by a Grant-in-Aid for Scientific Research (18002015) from the Ministry of Education, Culture, Sports, Science and Technology of Japan, a grant of the Program for Promotion of Fundamental Studies in Health Science from the National Institute of Biomedical Innovation of Japan and a grant from Ono Research Foundation.

AUTHOR CONTRIBUTIONS

Experimental design and discussion: T.O., T.M. and S.N.; performance of experiments and data analysis and interpretation: T.O. (for bleomycin experiments, cell culture and microarray analysis), T.M. (for promoter assays), C.Y. (for RT-PCR), K.N. (for microarray analysis and western blotting), S.K. (for X-gal staining), D.S. (for cell proliferation assays and flow cytometry), Y.K. and T.S. (for liquid chromatography–tandem mass spectrometry analysis), K.T. and Y.T. (for BALF from human subjects), K.C. and M.M. (for analysis of lung function); manuscript preparation: T.O., T.M. and S.N.

Published online at http://www.nature.com/naturemedicine/.
Reprints and permissions information is available online at http://npg.nature.com/reprintsandpermissions/.

1. Selman, M., King, T.E. & Pardo, A. Idiopathic pulmonary fibrosis: prevailing and evolving hypotheses about its pathogenesis and implications for therapy. *Ann. Intern. Med.* **134**, 136–151 (2001).
2. Border, W.A. & Noble, N.A. Transforming growth factor β in tissue fibrosis. *N. Engl. J. Med.* **331**, 1286–1292 (1994).
3. Munger, J.S. *et al.* The integrin αvβ6 binds and activates latent TGFβ1: a mechanism for regulating pulmonary inflammation and fibrosis. *Cell* **96**, 319–328 (1999).
4. Giri, S.N., Hyde, D.M. & Hollinger, M.A. Effect of antibody to transforming growth factor β on bleomycin induced accumulation of lung collagen in mice. *Thorax* **48**, 959–966 (1993).
5. Wang, Q. *et al.* Reduction of bleomycin induced lung fibrosis by transforming growth factor β soluble receptor in hamsters. *Thorax* **54**, 805–812 (1999).
6. Nakao, A. *et al.* Transient gene transfer and expression of Smad7 prevents bleomycin-induced lung fibrosis in mice. *J. Clin. Invest.* **104**, 5–11 (1999).
7. Kapoun, A.M. *et al.* Transforming growth factor-β receptor type 1 (TGFβRI) kinase activity but not p38 activation is required for TGFβRI-induced myofibroblast differentiation and profibrotic gene expression. *Mol. Pharmacol.* **70**, 518–531 (2006).
8. Nagase, T. *et al.* A pivotal role of cytosolic phospholipase A_2 in bleomycin-induced pulmonary fibrosis. *Nat. Med.* **8**, 480–484 (2002).
9. Hizaki, H. *et al.* Abortive expansion of the cumulus and impaired fertility in mice lacking the prostaglandin E receptor subtype EP2. *Proc. Natl. Acad. Sci. USA* **96**, 10501–10506 (1999).
10. Ushikubi, F. *et al.* Impaired febrile response in mice lacking the prostaglandin E receptor subtype EP3. *Nature* **395**, 281–284 (1998).
11. Segi, E. *et al.* Patent ductus arteriosus and neonatal death in prostaglandin receptor EP4-deficient mice. *Biochem. Biophys. Res. Commun.* **246**, 7–12 (1998).
12. Matsuoka, T. *et al.* Prostaglandin D_2 as a mediator of allergic asthma. *Science* **287**, 2013–2017 (2000).
13. Sugimoto, Y. *et al.* Failure of parturition in mice lacking the prostaglandin F receptor. *Science* **277**, 681–683 (1997).
14. Murata, T. *et al.* Altered pain perception and inflammatory response in mice lacking prostacyclin receptor. *Nature* **388**, 678–682 (1997).
15. Kabashima, K. *et al.* Thromboxane A_2 modulates interaction of dendritic cells and T cells and regulates acquired immunity. *Nat. Immunol.* **4**, 694–701 (2003).
16. Narumiya, S. Physiology and pathophysiology of prostanoid receptors. *Proc. Jpn. Acad. Ser. B.* **83**, 296–319 (2007).
17. Kabashima, K. *et al.* The prostaglandin receptor EP4 suppresses colitis, mucosal damage and CD4 cell activation in the gut. *J. Clin. Invest.* **109**, 883–893 (2002).
18. Kita, Y. *et al.* Pathway-oriented profiling of lipid mediators in macrophages. *Biochem. Biophys. Res. Commun.* **330**, 898–906 (2005).
19. Yoshikawa, K., Kita, Y., Kishimoto, K. & Shimizu, T. Profiling of eicosanoid production in the rat hippocampus during kainic acid–induced seizure: dual phase regulation and differential involvement of COX-1 and COX-2. *J. Biol. Chem.* **281**, 14663–14669 (2006).
20. Aono, Y. *et al.* Imatinib as a novel antifibrotic agent in bleomycin-induced pulmonary fibrosis in mice. *Am. J. Respir. Crit. Care Med.* **171**, 1279–1285 (2005).
21. DaCosta Byfield, S., Major, C., Laping, N.J. & Roberts, A.B. SB-505124 is a selective inhibitor of transforming growth factor-β type I receptors ALK4, ALK5 and ALK7. *Mol. Pharmacol.* **65**, 744–752 (2003).
22. Griffin, B.W., Klimko, P., Crider, J.Y. & Sharif, N.A. AL-8810: a novel prostaglandin $F_{2\alpha}$ analog with selective antagonist effects at the prostaglandin $F_{2\alpha}$ (FP) receptor. *J. Pharmacol. Exp. Ther.* **290**, 1278–1284 (1999).
23. Jinnin, M. *et al.* Potential regulatory elements of the constitutive up-regulated $\alpha 2_1$ collagen gene in scleroderma dermal fibroblasts. *Biochem. Biophys. Res. Commun.* **343**, 904–909 (2006).
24. Ihn, H. *et al.* Transcriptional regulation of the human $\alpha 2_1$ collagen gene. Combined action of upstream stimulatory and inhibitory cis-acting elements. *J. Biol. Chem.* **271**, 26717–26723 (1996).
25. Ishizaki, T. *et al.* Pharmacological properties of Y-27632, a specific inhibitor of rho-associated kinases. *Mol. Pharmacol.* **57**, 976–983 (2000).
26. Jinnin, M., Ihn, H. & Tamaki, K. Characterization of SIS3, a novel specific inhibitor of Smad3, and its effect on transforming growth factor-β1–induced extracellular matrix expression. *Mol. Pharmacol.* **69**, 597–607 (2006).
27. Ley, K. & Zarbock, A. From injury to fibrosis. *Nat. Med.* **14**, 20–21 (2008).
28. Bhatt, N. *et al.* Promising pharmacologic innovations in treating pulmonary fibrosis. *Curr. Opin. Pharmacol.* **6**, 284–292 (2006).
29. Border, W.A. & Noble, N.A. Targeting TGF-β for treatment of disease. *Nat. Med.* **1**, 1000–1001 (1995).
30. Wyss-Coray, T. *et al.* TGF-β1 promotes microglial amyloid-β clearance and reduces plaque burden in transgenic mice. *Nat. Med.* **7**, 612–618 (2001).
31. Moore, B.B. *et al.* Bleomycin-induced E prostanoid receptor changes alter fibroblast responses to prostaglandin E_2. *J. Immunol.* **174**, 5644–5649 (2005).
32. Lovgren, A.K. *et al.* COX-2–derived prostacyclin protects against bleomycin-induced pulmonary fibrosis. *Am. J. Physiol. Lung Cell. Mol. Physiol.* **291**, L144–L156 (2006).
33. Peters-Golden, M. *et al.* Protection from pulmonary fibrosis in leukotriene-deficient mice. *Am. J. Respir. Crit. Care Med.* **165**, 229–235 (2002).
34. Beller, T.C. *et al.* Targeted gene disruption reveals the role of the cysteinyl leukotriene 2 receptor in increased vascular permeability and in bleomycin-induced pulmonary fibrosis in mice. *J. Biol. Chem.* **279**, 46129–46134 (2004).
35. Tager, A.M. *et al.* The lysophosphatidic acid receptor LPA1 links pulmonary fibrosis to lung injury by mediating fibroblast recruitment and vascular leak. *Nat. Med.* **14**, 45–54 (2008).

ONLINE METHODS

Mice. We used female mice of 8–12 weeks of age. We generated mice lacking each prostaglandin receptor as chimeras of the 129SV and C57BL/6 backgrounds[9–15], backcrossed them for more than ten generations onto the C57BL/6 background except for *Ptger4*$^{-/-}$ mice and used them with WT C57BL/6 mice as a control. We maintained the mice on a 12-h light-dark cycle from in specific pathogen–free conditions. All experimental procedures were approved by the Committee on Animal Research of Kyoto University Faculty of Medicine.

Bleomycin-induced pulmonary fibrosis. We administered bleomycin (1 mg per kg body weight, Nippon Kayaku) in 40 μl saline intratracheally[8]. Control mice received saline alone. In one series of experiments, from one day after the bleomycin instillation, we gave mice 50 mg per kg body weight SD-208 (Tocris Bioscience) once daily in 0.2 ml of 1% methylcellulose or methylcellulose alone by gavage. For measurement of hydroxyproline content, we removed the lung from anesthetized mice and homogenized it in 1 ml of PBS. We mixed the homogenate with 1 ml HCl and incubated it at 110 °C overnight. We took a 10-μl aliquot and incubated it with chloramine-T solution (Wako Chemicals) for 20 min, followed by addition of Ehlich's reagent and incubation at 65 °C for 15 min. We measured absorbance at 590 nm in the final samples against a standard curve of hydroxyproline. For histology, we distended lungs by injection through the trachea of 10% formalin in PBS and then excised them. We embedded the tissue in paraffin, sliced it into sections and stained it with Masson's trichrome reagent. We evaluated lung function on day 21 by measuring lung elastance[8]. Briefly, we ventilated mice at a tidal volume of 0.3 ml and a frequency of 2.5 Hz with a Flexivent system (Scientific Respiratory Equipment). We measured the tracheal pressure, flow and volume, and we calculated lung elastance and resistance.

Mouse bronchoalveolar lavage fluid analysis. We cannulated the trachea and performed bronchoalveolar lavage with 1 ml PBS twice[8]. We spun the BALF at 450*g* for 10 min, and we saved the supernatant and the pellet separately. We resuspended the pellets and used an aliquot for counting the number of white blood cells on a hemocytometer. We cytospinned another aliquot of BALF cells and made differential leukocyte counts on a smear stained with Diff-Quick solution (International Reagents). We examined an aliquot of BALF cells on day 7 by flow cytometry after staining with either FITC-conjugated antibody to Thy1.2 and phycoerythrin-conjugated antibody to B220 eBioscience or FITC-conjugated antibody to CD4 and phycoerythrin-conjugated antibody to CD8 (eBioscience). We used the supernatant for determination of the amount of active TGF-β1 using a two-antibody sandwich ELISA kit (Promega) that detects a minimum of 31.3 pg ml^{-1} of TGF-β1 with less than 3% cross-reactivity to TGF-β2 and TGF-β3 at a concentration of 10 ng ml^{-1}.

Quantification of arachidonic acid metabolites. We obtained BAL samples from 15 subjects with IPF and 12 subjects with sarcoidosis by instillation with 150 ml sterile saline[36] after we obtained written informed consent from subjects and approval from the Institutional Ethical Committee of the Tenri Hospital. Because the subjects with sarcoidosis showed few signs of fibrosis with chest computed tomography, we used them as a control group. We centrifuged BALF to remove cellular components and stored it at −80 °C until use. We applied 1 ml of BALF to an extraction cartridge and used it for analysis. For the analysis of mouse lung, we anesthetized the mice and perfused them systemically via the heart with PBS. We dissected the left lung and immediately froze it under liquid nitrogen. We crushed frozen tissues to powder with an SK0100 mill (Tokken) and extracted them with 1 ml ethanol. We added a mixture of deuterium-labeled arachidonic acid metabolites as internal standards. We purified extracts with an Oasis HLB extraction cartridge. We performed quantification by liquid chromatography–electrospray ionization–tandem mass spectrometry as reported previously[18,19].

Cell culture experiments. We cultured primary cultures of lung fibroblasts, IMR90 and WI38 human fetal lung fibroblasts and LL29 human IPF lung fibroblasts as described in the **Supplementary Methods**.

Statistics. Data are expressed as means ± s.e.m. We made comparisons among data with either Student's *t* test or analysis of variance with a *post hoc* Scheffe's or Dunnett's test. We considered *P* values of less than 0.05 statistically significant.

Additional methods. Collagen production assay, quantitative real-time RT-PCR, proliferation assay and promoter assay are described in the **Supplementary Methods**.

36. Handa, T. *et al.* Polymorphisms of B7 (CD80 and CD86) genes do not affect disease susceptibility to sarcoidosis. *Respiration* **72**, 243–248 (2005).

Biochemical and Biophysical Research Communications 389 (2009) 580–585

Contents lists available at ScienceDirect

Biochemical and Biophysical Research Communications

journal homepage: www.elsevier.com/locate/ybbrc

Solution structure of the *E. coli* ribosome hibernation promoting factor HPF: Implications for the relationship between structure and function

Akiko Sato [a], Takumi Watanabe [a], Yasushi Maki [b], Masami Ueta [b,c], Hideji Yoshida [b], Yutaka Ito [a], Akira Wada [c], Masaki Mishima [a,*]

[a] Graduate School of Science and Technology, Tokyo Metropolitan University, 1-1 Minamiosawa, Hachioji 192-0397, Japan
[b] Department of Physics, Osaka Medical College, Takatsuki, Osaka, 569-8686, Japan
[c] Yoshida Biological Laboratory, Yamashina, Kyoto 607-8081, Japan

ARTICLE INFO

Article history:
Received 28 August 2009
Available online 10 September 2009

Keywords:
Hibernation promoting factor
HPF
YfiA
RMF
NMR
100S ribosome
Structure

ABSTRACT

The 70S *Escherichia coli* ribosome dimerizes to form an inactive 100S ribosome during stationary phase, which is called "ribosome hibernation". The hibernation promoting factor HPF plays a crucial role in 100S ribosome formation. However, YfiA, a known paralog of HPF inhibits 100S formation, although it shares high sequence similarity. Here, we report the first solution structure of HPF as determined by multi-dimensional NMR. HPF adopts βαββββα-fold and the overall structure is similar to YfiA as expected. However, detailed structure comparison based on the determined structure in this study revealed that there are remarkable differences around the C-terminal portion of helix α2, which is not predicted by homology modeling. Furthermore, some acidic residues conserved only in HPF are located at the rim of the common basic patch.

Introduction

During prolonged culture, the exponential phase of growth shifts to the stationary phase. Morphological and physiological properties of bacterial cells, and expression levels of many proteins are changed with a transition from the exponential phase to the stationary phase. In *Escherichia coli*, dimerization of 70S ribosomes result in the formation of 100S ribosomes, which are formed in the stationary phase [1] and have no translational activity [2]. This 100S formation is referred to as ribosome hibernation [3]. Of particular note is that ribosomal binding proteins such as RMF, YfiA, HPF [4] and SRA [5], are expressed throughout the stationary phase implying that these four proteins play important roles during the stationary phase in *E. coli*.

RMF is a small basic protein and its expression increases significantly during the stationary phase [6]. RMF binds to ribosomes and inactivates translation, which, in part, also causes 70S ribosome dimerization. RMF binding sites on the *E. coli* 23S rRNA have been identified by chemical probing methods using dimethyl sulphate, and found to be in the vicinity of the PTase center [3,7].

In addition to the binding of RMF to the ribosomes, HPF has been found to be associated with the dimerized ribosomes in the stationary phase. Intriguingly, YfiA, an HPF paralog sharing 40% sequence homology, is also expressed in the stationary phase and binds to the ribosomes, but is found mainly in the monomeric 70S fraction [4]. YfiA is also known as Protein Y, which binds to the 70S ribosome and inhibits translation during cold shock [8,9]. The functions of HPF and YfiA in the *in vivo* formation of 70S dimers have been examined using deletion mutants of HPF and YfiA [10]. YfiA deletion mutant expressing both HPF and RMF formed a large number of 100S ribosomes than the wild type during the stationary phase, suggesting that YfiA regulates 100S formation in a negative manner. In contrast, the HPF deletion mutant expressing both YfiA and RMF was not able to form the 100S dimer indicating that HPF plays a key role in 100S formation.

A recent crystallographic study has shown that YfiA bind to the 30S subunit at the P-site and A-site, close to the interface between the 50S and the 30S subunits [9]. Although, washing with high salt buffer does not remove HPF and YfiA from either the 70S or 100S ribosome, low magnesium treatment, which dissociates the 70S ribosome into 30S and 50S subunits, successfully results in the release of HPF and YfiA from the ribosome [4]. These data indicate that association between large and small subunits is important for efficient binding HPF and YfiA to the ribosome. Recently, it has been shown that ribosomal dissociation activity by IF3 is

Abbreviations: NOE, nuclear overhauser effect; NOESY, NOE spectroscopy; TOCSY, total correlation spectroscopy; HSQC, heteronuclear single quantum correlation spectroscopy; r.m.s., root mean square.

* Corresponding author. Fax: +81 42 677 2525.
E-mail address: mishima-masaki@tmu.ac.jp (M. Mishima).

0006-291X/$ - see front matter © 2009 Elsevier Inc. All rights reserved.
doi:10.1016/j.bbrc.2009.09.022

decreased and thus ribosomal dimerization activity by RMF and HPF is elevated in the stationary phase by *in vitro* analyses [11].

Data base searches and phylogenetic analysis showed that there are three classes of HPF homologue: short HPF, long HPF and YfiA [12]. Short HPF, which has no C-terminal extension, is found in gamma and beta proteobacteria, while long HPF, which has a long tail region at the C-terminus, is found in the other bacteria and plant plastids. Intriguingly, YfiA, which has a short extension of the C-terminus, and RMF are found only in gamma proteobacteria.

More specifically, gamma proteobacteria possess short HPF, YfiA and RMF, while other bacteria which possess long HPF do not carry RMF and YfiA [12]. These data imply that long HPF may regulate translation by itself, while RMF, short HPF and YfiA coordinately regulate translation.

As a first step in understanding the complicated mechanism of 100S formation, we determined the tertiary structure of HPF. Herein, we report the solution structure of the *E. coli* HPF, a member of the short HPF family, as determined by heteronuclear multidimensional NMR. To the best of our knowledge, this is the first description of the tertiary structure of HPF.

Materials and methods

Sample preparation. HPF was expressed in *E. coli* M15 cells harboring the plasmid pQE9 encoding HPF. Uniform labeling of proteins with ^{15}N or ^{15}N and ^{13}C was achieved using M9 minimal medium containing $^{15}NH_4Cl$ and [$^{13}C_6$]-glucose as the sole source of nitrogen and carbon, respectively. Cells were grown at 37 °C, and protein expression induced by IPTG when the A_{660nm} was 0.5. Post-induction, cells were cultured at 20 °C and harvested 16 hrs later. Harvested wet cells were resuspended in 50 mM HEPES buffer (pH 7.5) containing 400 mM KCl and 0.1 mM EDTA. The suspension was lysed by sonication, and ultra-centrifuged. The supernatant was then loaded onto DEAE-Sepharose. The flow-through fraction was collected, and salt-cut was performed by 30% saturated $(NH_4)_2SO_4$. The protein was further purified with the aid of a Superdex-75 gel filtration column (GE Healthcare). Sample homogeneity was checked by SDS–PAGE.

NMR spectroscopy and structure calculation of HPF. Purified HPF was dissolved in 50 mM K-phosphate buffer (pH 6.9) containing 20 mM KCl and 0.1 mM EDTA in either 93% H_2O/7% ^2H_2O or 99.8% ^2H_2O. The final concentration of the protein was around 1 mM. NMR spectra were acquired at 30 °C on a Bruker AVANCE 600 NMR spectrometer equipped with a cryogenic probe. Non-uniformly sampled (NUS) data were processed by Azara version 2.7 (Boucher, W., http://www.ccpn.ac.uk/azara). Other conventional type data were processed by NMRPipe version 3.0 [13]. Data processed by Azara were converted to NMRPipe format using Olivia version 1.14 (Yokochi, M., Sekiguchi, S. and Inagaki, F., Hokkaido University, Sapporo, Japan), and the obtained spectra analyzed using Sparky (Goddard, T.D. and Kneller, D.G., University of California, San Francisco, CA). The ^1H, ^{13}C, and ^{15}N assignments were mainly obtained from standard multi-dimensional NMR methods [14], NUS-CBCANH, NUS-CBCA(CO)NH, NUS-HN(CA)CO, and NUS-HNCO for main-chain assignments, and C(CO)NH, H(CCO)NH, HCCH-TOCSY, and 4D HC(CO)NH [15] for side-chain assignments. Inter-proton distances were derived from 3D ^{15}N edited NOESY-HSQC, 4D $^{13}C/^{15}N$ edited HMQC-NOESY-HSQC and 3D ^{13}C edited NOESY-HSQC. Backbone dihedral φ and ψ angles were derived from TALOS [16]. The $\chi 1$ rotomer of the side-chains was estimated from HNHB and HN(CO)HB experiments [17,18]. Residual $^1D_{NH}$ couplings were obtained by comparison with the ^{15}N–^1H couplings obtained from isotropic and anisotropic samples. The couplings were measured by using HNCO-TROSY experiments performed in an interleaved manner [19]. The anisotropic sample contained 15 mg/ml pf1 phage.

The program CYANA version 3.00, using the CANDID protocol, was used for structural restraint collection [20]. Finally, an ensemble of 100 HPF structures were calculated using the program CNS version 1.2 with residual $^1D_{NH}$ couplings by a standard simulated annealing protocol [21]. Initial estimation for the axial component of molecular alignment tensor (Da) and rhombicity (R) were obtained based on the structure calculated by CYANA. These values were optimized in an iterative manner. The final values of Da and R were 7.9 Hz and 0.59, respectively. The final lowest energy 20 ensemble structures were checked by PROCHECK-NMR [22], and graphics created by MOLMOL [23] and PyMOL (DeLano Scientitilc. San Carlos, CA). The lowest energy structure among the ensemble was used as a representative in order to compare structure, generate a ribbon model, and calculate an electrostatic potential map using APBS [24].

Results and discussion

Structure determination of HPF

Purified HPF provided well-dispersed ^1H–^{15}N HSQC spectrum (Supplementary data Fig. S1). The elution volume from gel-filtration corresponded to the molecular weight of the monomer, and the NMR spectral line shape was relatively narrow. These data indicated that HPF exists as a monomer in solution. Almost all ^1H, ^{13}C, and ^{15}N NMR signals were assigned using standard multi-dimensional NMR techniques. Non-uniform sampling (NUS)

Table 1[a]

Total number of distance constraints	2300
Long range (|*i*–*j*| > 4)	635
Middle range (|*i*–*j*| = 2,3,4)	449
Short range (|*i*–*j*| = 1)	471
Intra residue	677
Hydrogen bond constraints	34 × 2
Dihedral constraints	
ϕ, φ	87,87
X_1	28
Residual dipole couplings	
^{1}Dnh	75
R.m.s. deviation from experimental restraints[b]	
Distance (A)	0.008 ± 0.0007
Angle (°)	0.44 ± 0.08
^{1}Dnh (Hz)	0.36 ± 0.03
Q-factor for experimental residual dipolar coupling restraints	
$^1D_{NH}$	0.036 ± 0.002
R.m.s. deviation from idealized covalent geometry	
Bonds (A)	$0.0011 \pm 6x10^{-5}$
Angles (°)	0.311 ± 0.007
Impropers (°)	0.166 ± 0.01
CNS energy terms (kcal/mol)[c]	
E_{bond}	1.72 ± 0.18
E_{angle}	41.0 ± 1.8
E_{imp}	3.29 ± 0.56
$E_{vdw(LJ)}$	−306 ± 8
PROCHECK Ramachandran plot (1–89)	
Residues in most favoured regions (%)	91.5
Residues in additional allowed regions (%)	7.6
Residues in generously allowed regions (%)	0.4
Residues in disallowed regions (%)	0.5
R.m.s. deviation of mean structure derived from 20 calculated structures	
Back bone (1–89) (Å)	0.39
All heavy (1–89) (Å)	0.84

[a] These statistics comprise the ensemble of the 20 lowest energy structures obtained from 100 starting structures. Structure calculations were performed using CNS version 1.2.

[b] None of these structures exhibited distance violations >0.4 Å, dihedral angle violations > 5° and residual $^1D_{NH}$ dipolar coupling violations >1.1 Hz.

[c] E_{vdw} is the Lennerd-Jones energy of CNS energy terms.

facilitated efficient data collection for the resonance assignments. The numbers of distance restraints derived from NOEs were sufficient (more than two thousand), and 75 N–H residual dipole couplings were also used (Table 1). Fig. 1A depicts the back bone of the final 20 structures derived from NMR data showing that the atomic coordinates throughout the protein molecule have been well defined, with the exception of the C-terminal five residues (90–94). The average r.m.s. deviations calculated from the averaged structure were 0.39 and 0.84 Å for the back bone and all heavy atoms of the well-defined region (residues 1–89), respectively. Statistical data for the structures are given in Table 1.

Structure of the HPF

HPF adopts a βαββββα-fold, comprised of a layer of mixed parallel and anti-parallel β-sheet, and two α-helices. The β-sheet is composed of β1 (residues 1–7), β2 (35–41), β3 (47–55) and β4 (58–66),

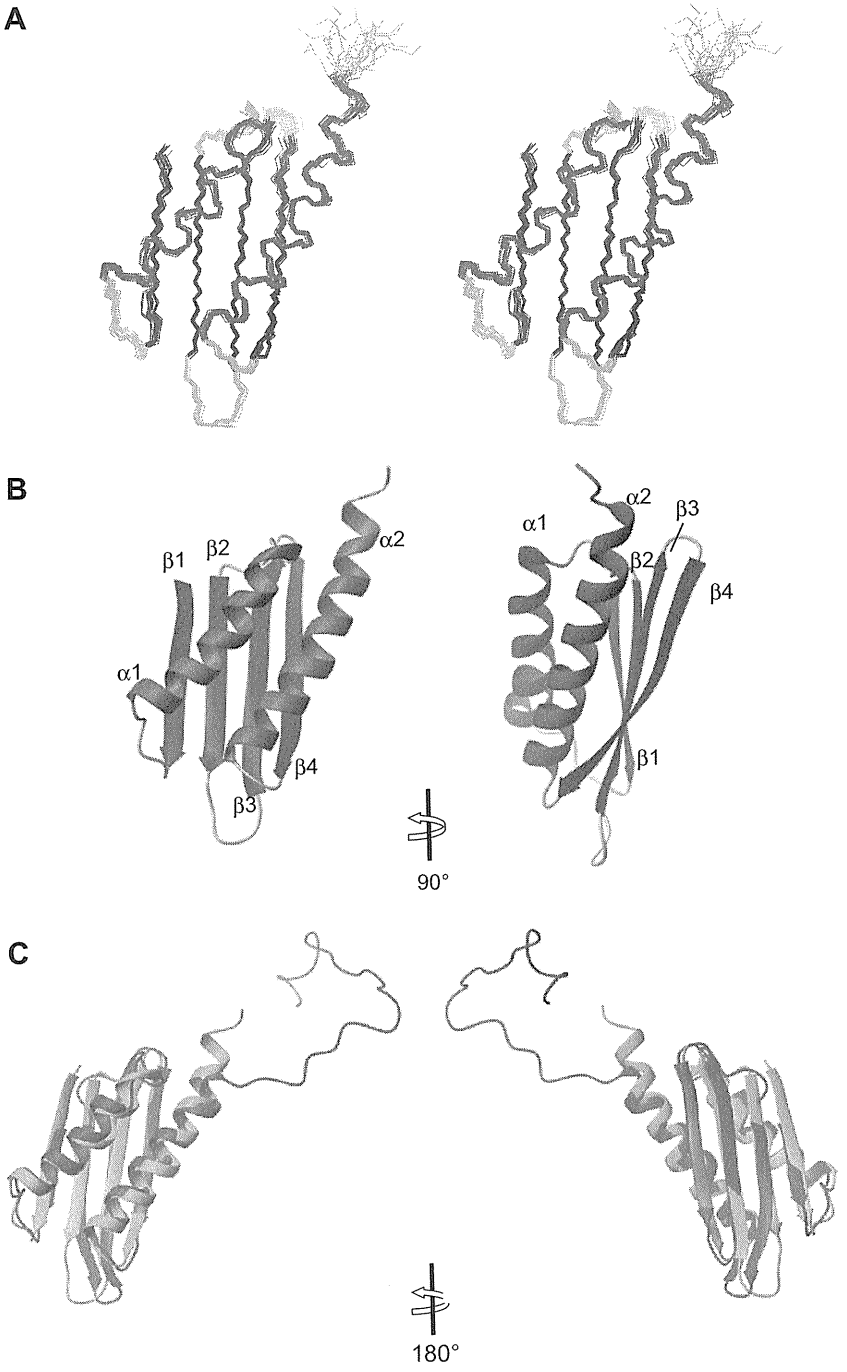

Fig. 1. Solution structure of HPF. (A) Stereo view of the backbone superposition of the final 20 simulated annealing structures. Helices and strands are shown in red and blue, respectively. (B) Ribbon drawing of the representative structure of HPF in two different views. The molecular orientation in the *left-hand image* is the same as in (A), and the four stranded β-sheet and α-helices are depicted in blue and red, respectively. The *right-hand image* was obtained by 90° rotation of the *left-hand image* about the horizontal axis. (C) Structure comparison of HPF and YfiA. Ribbon models of HPF and YfiA are colored in cyan and magenta, respectively.

and is backed by α-helices α1 (13–29) and α2 (69–91) (Fig. 1B). As expected from the high sequence similarity, the overall structure of HPF resembles that of YfiA showing a high *Z*-score (Fig. 1C), around 13–11, according to a DALI database search [25–27]. Z-scores of YfiA structures, are 13.8, 12.9, 11.8 11.5 and 11.4 for PDB code 2YWQ, 1VOZ, 1IMU, 1L4S, 1N3G, respectively. The r.m.s. deviation between HPF and YfiA (PDB code: 1L4S) is 1.4 Å for the back bone coordinates in the secondary structure region (residues 1–7, 35–41, 47–55, 58–66, 13–29, 69–88).

Conserved hydrophobic residues among HPFs and YfiAs are likely to play a key role in forming the tertiary structure. Fig 2 shows hydrophobic interactions within the protein core of HPF. Hydrophobic residues, Leu2 and Ile4 on the β1, Val36, Val38 and Leu40 on the β2, Ala51 and Leu53 on the β3, and Ile60 and Ala62 on the β4 are inward facing residues on the β-sheet. Hydrophobic residues on the α-helices pack the hydrophobic core of the β-sheet, namely: Leu15, Val19, Phe23, Leu26 and Phe30 on the α1, and Met69, Ile73, Leu76, Ile77, Leu80 and Leu84 on the α2. These hydrophobic residues are conserved throughout between HPF and YfiA except for Phe30 (Fig. S2), which contributes to the common fold between HPF and YfiA.

Notably, the aromatic ring of Phe30 interacts with aliphatic β-methylene of Leu84 in the determined HPF structure (Fig 2). In NMR measurements, the ^{1}H signals of these β-methylenes are well separated, implying that the side-chain of Leu84 adopts a well-defined conformation. The signals show up-field shift, possibly due to ring current effect (chemical shifts of the signals are 0.83 and 1.45 ppm, respectively). This confirmed the interaction between the aromatic ring of Phe30 and the β-methylene of Leu84.

Functional implications

The structure of YfiA in complex with the 70S ribosome was recently reported. Key residues for interaction with the ribosome were suggested in the literature, although the resolution was low, 11 Å [9]. YfiA bound to the 30S subunit of the 70S ribosome overlapping with the binding site of anticodon stems of A- and P- site tRNAs. In the literature, Arg22, Lys25, Lys28, Lys79, Arg82, and Lys86 were suggested as key residues for ribosome binding. Three basic residues (Lys79, Arg82, and Lys86), exposed on the helix α2, approached the bases of conserved P-site residues of the ribosome, whereas Arg22, Lys25, and Lys28 residues are located in the vicinity of the phosphate back bone of the P- and A-site. These residues are conserved in HPF, corresponding residues being Lys22, Lys25, Lys79, Arg82, and Lys86, with the exception of Gln28 which loses positive charge of the side-chain (Figs. S2 and 3A). Spatial arrangements of these residues in the determined structure of HPF are identical to that of the previously determined structure of YfiA [26,27].

An electrostatic potential map of the molecular surface of HPF is shown in Fig. 3B. Notably, the aforementioned Lys22, Lys25, Lys79, Arg82, and Lys86, form a small basic patch, even despite the fact that HPF is an acidic protein. A similar basic patch also exists in YfiA indicating that both HPF and YfiA adopt a similar mechanism for ribosome binding. This supports the hypothesis that HPF and YfiA share the same binding region on the ribosome.

The most striking difference between the structures is the existence of a flexible 18 residue C-terminal extension following helix α2 in YfiA, which is missing in HPF (Fig. 1C). It should be noted that the *E. coli* HPF investigated in this study belongs to short HPF, which exerts a coordinating mode of action with RMF, while YfiA has a C-terminal extension. Thus, the hypothesis that RMF plays a complementary role by compensating for the absence of the extension is attractive. By assuming heterodimer formation of HPF and RMF in coordinate modes of action, we have investigated the interaction between HPF and RMF. Chemical shift perturbation experiments monitoring the chemical shift changes following the addition of RMF have been attempted, but perturbations of the NMR signals have not been observed (data not shown). This means that RMF does not directly interact with HPF in solution. However, the possible HPF binding site for the ribosome, deduced from comparison with the 70S ribomsome-YfiA complex structure, and the RMF binding site for the ribosome revealed by chemical foot printing, are juxtaposed. HPF and RMF may interact with each other on the ribosome and play a coordinating function. RMF consists of 50 residues and is thus longer than the C-terminal extension of YfiA. Thereby, coordinate action of HPF and RMF could potentially cause more significant structural changes around the ribosome PTase center, and following allosteric effects may result in the formation of the 100S ribosome.

Other than C-terminal extension, there are notable structural differences between HPF and YfiA. Intriguingly, the exposed residues Asp31 and Lys88 are conserved only in HPF (Fig. 3A). They locate closely in the NMR structure, suggesting the existence of a possible salt bridge (Fig. 3A). Furthermore, the aforementioned

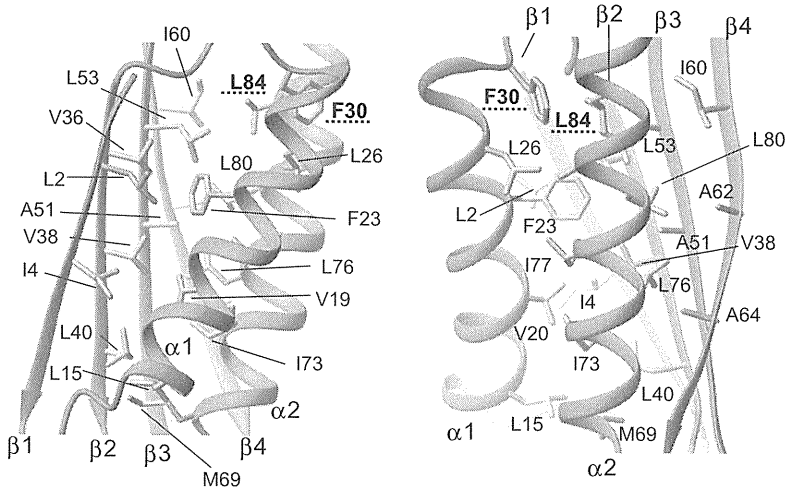

Fig. 2. Hydrophobic interactions mediated by conserved residues. Hydrophobic residues conserved in both HPF and YfiA, which mediate contacts among inward facing residues. Their side-chains are shown by stick models in yellow. Phe30 and Leu84 are shown in bold and marked by dotted line.

hydrophobic residue Phe30 is conserved only with HPF buried in the hydrophobic core (Fig. 2). These interactions stabilize the C-terminal part of helix α2. Consequently, the C-terminal part of helix α2 of HPF is longer, by one turn, than that of YfiA (Fig 1C). Generally, HPF has a rigid and well-stabilized structure around helix α2. It should be noted that this specific character in the HPF structure is not predicted by a standard homology modeling approach based on the YfiA structure. Since homology model is built from a template tertiary structure, more stabilized structure and an additional ordered structure in a target are hardly predicted.

Meanwhile, the surface exposed acidic residues, Glu59, Asp74, Asp78, and Asp89, are also conserved in HPF only (Figs. S2 and 3A). Notably, Asp74, Asp78, and Asp89 are located on the rim of the basic patch formed by Lys22, Lys25, Lys79, Arg82, and Arg86, and may also contribute to the specific function of HPF (Fig. 3A and B). Specifically, HPF and YfiA may bind to the ribosome in a similar manner via the basic patch and conserved basic residues, and the functional differences of HPF and YfiA are most likely to be caused by differences at the C-terminus, and the acidic residues around the basic patch. Of note, Glu10, Glu43, and Asp50 are also conserved in HPF (Fig. S2) and exposed on the protein surface, but they are conserved in both HPF and YfiA, and they do not contribute the interaction with the ribosome in the 70S ribomsome–YfiA complex structure. Thus, those three residues may not be important. These observation and hypotheses derived from this study provide the clues for next functional studies to address the regulation mechanism of ribosomes by HPF and YfiA. Functional studies using chimera proteins between HPF and YfiA, in which the C-terminal extension and the acidic residues conserved only in HPF are swapped or deleted, are attractive.

Conclusion

We have determined the first tertiary structure of HPF. While the similarity in overall structure between HPF and YfiA, and the conservation of spatial arrangements for possible ribosome binding residues, suggest similar binding mechanisms, we found that HPF exhibits a specific structural character based on the determined HPF structure in this study. Instead of the absence of a C-terminal extension, the helix α2 is well stabilized and some conserved acidic residues are exposed at the rim of the common basic patch. These structural differences between HPF and YfiA, and the coordinating action with RMF may exert different functional effects compared to YfiA.

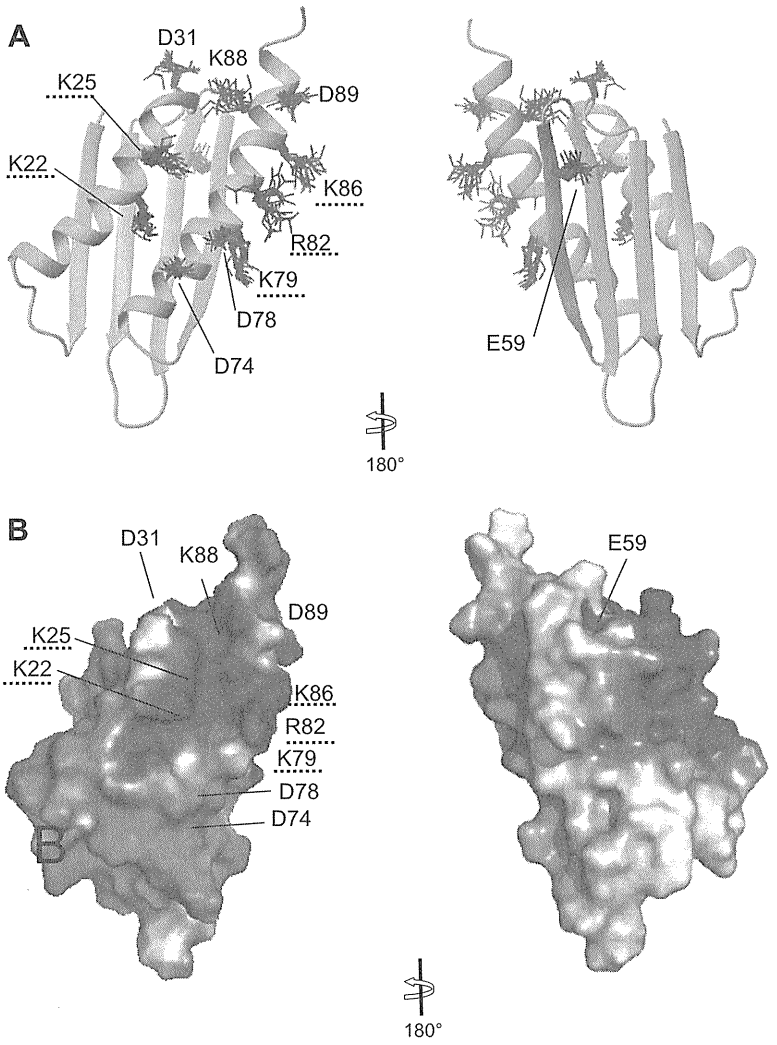

Fig. 3. Surface exposed conserved residues. (A) Basic and acidic residues are colored in blue and red, respectively. Of these, the residues conserved in both HPF and YfiA, which contribute ribosome binding in the ribomsome-YfiA complex structure [9], are marked by dotted line. (B) Electrostatic potential mapped on the molecular surface of HPF. The molecular orientations are the same as in (A).

Acknowledgments

We thank Teppei Kanaba for critical reading of the manuscript and technical assistance, and Yoshitaka Nagai for help with sample preparation. This work was supported in part by Grants-in-Aid for Scientific Research to M.M. from the Ministry of Education, Culture, Sports, Science, and Technology (MEXT) of Japan, and Grants-in-Aid for Scientific Research on Priority Areas 'Spatio-temporal Network of RNA Information Flow' (20 570 167) from the MEXT of Japan to H.Y.

Appendix A. Supplementary data

Supplementary data associated with this article can be found, in the online version, at doi:10.1016/j.bbrc.2009.09.022.

References

[1] A. Wada, Y. Yamazaki, N. Fujita, A. Ishihama, Structure and probable genetic location of a "ribosome modulation factor" associated with 100S ribosomes in stationary-phase *Escherichia coli* cells, Proc. Natl. Acad. Sci. USA 87 (1990) 2657–2661.
[2] A. Wada, K. Igarashi, S. Yoshimura, S. Aimoto, A. Ishihama, Ribosome modulation factor: stationary growth phase-specific inhibitor of ribosome functions from *Escherichia coli*, Biochem. Biophys. Res. Commun. 214 (1995) 410–417.
[3] H. Yoshida, Y. Maki, H. Kato, H. Fujisawa, K. Izutsu, C. Wada, A. Wada, The ribosome modulation factor (RMF) binding site on the 100S ribosome of *Escherichia coli*, J. Biochem. 132 (2002) 983–989.
[4] Y. Maki, H. Yoshida, A. Wada, Two proteins, YfiA and YhbH, associated with resting ribosomes in stationary phase *Escherichia coli*, Genes Cells 5 (2000) 965–974.
[5] K. Izutsu, C. Wada, Y. Komine, T. Sako, C. Ueguchi, S. Nakura, A. Wada, *Escherichia coli* ribosome-associated protein SRA, whose copy number increases during stationary phase, J. Bacteriol. 183 (2001) 2765–2773.
[6] K. Izutsu, A. Wada, C. Wada, Expression of ribosome modulation factor (RMF) in *Escherichia coli* requires ppGpp, Genes Cells 6 (2001) 665–676.
[7] H. Yoshida, H. Yamamoto, T. Uchiumi, A. Wada, RMF inactivates ribosomes by covering the peptidyl transferase centre and entrance of peptide exit tunnel, Genes Cells 9 (2004) 271–278.
[8] D.E. Agafonov, V.A. Kolb, A.S. Spirin, Ribosome-associated protein that inhibits translation at the aminoacyl-tRNA binding stage, EMBO Rep. 2 (2001) 399–402.
[9] A. Vila-Sanjurjo, B.S. Schuwirth, C.W. Hau, J.H. Cate, Structural basis for the control of translation initiation during stress, Nat. Struct. Mol. Biol. 11 (2004) 1054–1059.
[10] M. Ueta, H. Yoshida, C. Wada, T. Baba, H. Mori, A. Wada, Ribosome binding proteins YhbH and YfiA have opposite functions during 100S formation in the stationary phase of *Escherichia coli*, Genes Cells 10 (2005) 1103–1112.
[11] H. Yoshida, M. Ueta, Y. Maki, A. Sakai, A. Wada, Activities of *Escherichia coli* ribosomes in IF3 and RMF change to prepare 100S ribosome formation on entering the stationary growth phase, Genes Cells 14 (2009) 271–280.
[12] M. Ueta, R.L. Ohniwa, H. Yoshida, Y. Maki, C. Wada, A. Wada, Role of HPF (hibernation promoting factor) in translational activity in *Escherichia coli*, J. Biochem. 143 (2008) 425–433.
[13] F. Delaglio, S. Grzesiek, G.W. Vuister, G. Zhu, J. Pfeifer, A. Bax, NMRPipe: a multidimensional spectral processing system based on UNIX pipes, J. Biomol. NMR 6 (1995) 277–293.
[14] M. Sattler, J. Schleucher, C. Griesinger, Heteronuclear multidimensional NMR experiments for the structure determination of proteins in solution employing pulsed field gradients, Prog. Nuclear Magn. Reson. Spectrosc. 34 (1999) 93–158.
[15] R.T. Clowes, W. Boucher, C.H. Hardman, P.J. Domaille, E.D. Laue, A 4D HCC(CO)NNH experiiment for the correlation of aliphatic side-chain and backbone resonances in $^{13}C/^{15}N$-labelled proteins, J. Biomol. NMR 3 (1993) 349–354.
[16] G. Cornilescu, F. Delaglio, A. Bax, Protein backbone angle restraints from searching a database for chemical shift and sequence homology, J. Biomol. NMR 13 (1999) 289–302.
[17] S.J. Archer, M. Ikura, D.A. Torchia, A. Bax, An alternative 3D NMR technique for correlating backbone 15N with side-chain Hb resonances in larger proteins, J. Magn. Reson. 95 (1991) 636–641.
[18] S. Grzesiek, M. Ikura, G.M. Clore, A.M. Gronenborn, A. Bax, A 3D triple-resonance NMR technique for qualitative measurement of carbonyl-Hb *J* couplings in isotopically enriched protein, J. Magn. Reson. 96 (1992) 215–221.
[19] Y. Daiwen, V.A. Ronald, A.M. Geoffrey, W.Y. Choy, L.E. Kay, TROSY-based HNCO pulse sequences for the measurement of $^{1}HN-^{15}N$, $^{15}N-^{13}CO$, $^{1}HN-^{13}CO$, $^{13}CO-^{13}C\alpha$ and $^{1}HN-^{13}C\alpha$ dipolar couplings in ^{15}N, ^{13}C, ^{2}H-labeled proteins Journal of Biomolecular NMR 14 (1999) 333–343.
[20] T. Herrmann, P. Guntert, K. Wuthrich, Protein NMR structure determination with automated NOE assignment using the new software CANDID and the torsion angle dynamics algorithm DYANA, J. Mol. Biol. 319 (2002) 209–227.
[21] A.T. Brunger, P.D. Adams, G.M. Clore, W.L. DeLano, P. Gros, R.W. Grosse-Kunstleve, J.S. Jiang, J. Kuszewski, M. Nilges, N.S. Pannu, R.J. Read, L.M. Rice, T. Simonson, G.L. Warren, Crystallography & NMR system: A new software suite for macromolecular structure determination, Acta Crystallogr. D 54 (1998) 905–921.
[22] R.A. Laskowski, J.A. Rullmannn, M.W. MacArthur, R. Kaptein, J.M. Thornton, AQUA and PROCHECK-NMR: programs for checking the quality of protein structures solved by NMR, J. Biomol. NMR 8 (1996) 477–486.
[23] R. Koradi, M. Billeter, K. Wuthrich, MOLMOL: a program for display and analysis of macromolecular structures, J. Mol. Graph. 14 (1996) 51–55.
[24] N.A. Baker, D. Sept, S. Joseph, M.J. Holst, J.A. McCammon, Electrostatics of nanosystems: application to microtubules and the ribosome, Proc. Natl. Acad. Sci. USA 98 (2001) 10037–10041.
[25] L. Holm, C. Sander, Mapping the protein universe, Science 273 (1996) 595–603.
[26] A. Rak, A. Kalinin, D. Shcherbakov, P. Bayer, Solution structure of the ribosome-associated cold shock response protein Yfia of *Escherichia coli*, Biochem. Biophys. Res. Commun. 299 (2002) 710–714.
[27] K. Ye, A. Serganov, W. Hu, M. Garber, D.J. Patel, Ribosome-associated factor Y adopts a fold resembling a double-stranded RNA binding domain scaffold, Eur. J. Biochem. 269 (2002) 5182–5191.

CHEST

Original Research

COPD

CT Scan Findings of Emphysema Predict Mortality in COPD

Akane Haruna, MD; Shigeo Muro, MD, PhD; Yasutaka Nakano, MD, PhD; Tadashi Ohara, MD, PhD; Yuma Hoshino, MD, PhD; Emiko Ogawa, MD, PhD; Toyohiro Hirai, MD, PhD; Akio Niimi, MD, PhD; Koichi Nishimura, MD, PhD; Kazuo Chin, MD, PhD; and Michiaki Mishima, MD, PhD

Background: **Emphysematous change as assessed by CT imaging has been reported to correlate with COPD prognostic factors such as FEV_1 and diffusing capacity of the lung for carbon monoxide (DLCO). However, few studies have assessed the relationship between CT scan assessment and COPD mortality from mild to severe stages of the disease. In this study, we analyzed this relationship in patients with various stages of COPD.**

Methods: **Two hundred and fifty-one outpatients with stable COPD were included in the study. CT scan and pulmonary function tests were performed at study entry in a single institution. The percentage of low attenuation area was measured to quantitatively evaluate emphysematous change with a custom-made software. Prognostic data also were collected, and the median follow-up time was 8 years.**

Results: **Of the 251 patients, 79 died, with 40 classified as respiratory deaths not involving lung cancer. Univariate Cox analysis revealed that emphysematous change as assessed by CT scan, lung function, age, or BMI were significantly correlated with mortality. Multivariate analysis revealed that emphysematous change as assessed by CT scan had the best association with mortality.**

Conclusions: **Emphysematous change as assessed by CT scan predicts respiratory mortality in outpatients with various stages of COPD.** ***CHEST 2010; 138(3):635–640***

Abbreviations: AATD = α-1-antitrypsin deficiency; DLCO = diffusing capacity of the lung for carbon monoxide; GOLD = Global Initiative for Chronic Obstructive Lung Disease; HR = hazard ratio; HU = Hounsfield units; LAA = low attenuation areas; LAA% = the percentage of the lung field occupied by low attenuation areas; NETT = National Emphysema Treatment Trial; PFT = pulmonary function test; RV/TLC = residual volume/total lung capacity; VA = alveolar volume

COPD is one of the leading causes of death worldwide.[1] Investigating the factors that influence COPD mortality, therefore, is of great importance for improving world health problems. Numerous factors already have been reported to influence COPD prognosis, including age,[2-4] FEV_1,[3,5,6] diffusing capacity of the lung for carbon monoxide (DLCO),[4] hypoxemia,[7,8] pulmonary hypertension,[9] BMI,[4,10,11] breathlessness,[2,12] and impaired exercise capacity.[4,13]

We have shown that the extent of emphysematous change as assessed by CT images quantified with a custom-made software correlated with several

Manuscript received November 29, 2009; revision accepted March 22, 2010.

Affiliations: From the Department of Respiratory Medicine (Drs Haruna, Muro, Hoshino, Ogawa, Hirai, Niimi, and Mishima), Graduate School of Medicine, Kyoto University, Kyoto; Department of Respiratory Medicine (Dr Nakano), Shiga University of Medical Science, Otsu, Shiga; Kariya Toyota General Hospital (Dr Ohara), Kariya, Aichi; Department of Respiratory Medicine (Dr Nishimura), Murakami Memorial Hospital, Asahi University, Gifu; and Department of Respiratory Care and Sleep Control Medicine (Dr Chin), Graduate School of Medicine, Kyoto University, Kyoto, Japan.

Funding/Support: This study was partially supported by a Grant-in-Aid for scientific research (B) [No. 16390234] and (C) [No. 21590964].

Correspondence to: Shigeo Muro, MD, PhD, Department of Respiratory Medicine, Graduate School of Medicine, Kyoto University, 54 Shogoin-Kawahara-cho, Sakyo-ku, Kyoto 606-8507, Japan; e-mail: smuro@kuhp.kyoto-u.ac.jp

DOI: 10.1378/chest.09-2836

prognostic factors, such as FEV_1,[14] DLCO,[14] and BMI.[15] Consequently, the severity of emphysema is itself expected to be a prognostic factor for mortality. Indeed, in patients with α-1-antitrypsin deficiency (AATD), the extent of emphysema, as measured by CT imaging, was reported to be a stronger predictor of mortality than other factors.[16] Martinez et al[17] found that this was not the case for patients with COPD without AATD, although their patient population was clustered at the severe end of the disease spectrum. In an ordinary clinical setting, clinicians see patients with COPD of various degrees of severity, and AATD and candidacy for lung volume reduction surgery are less common. Therefore, we investigated the relationship between the extent of emphysematous change as measured by CT imaging and mortality in patients with COPD with varying degrees of disease severity.

Materials and Methods

Subjects and Study Design

This study is part of an ongoing COPD follow-up study being performed at Kyoto University (Kyoto, Japan). From regularly treated outpatients with COPD, 251 were enrolled who had CT scans performed at Kyoto University Hospital between April 1995 and April 2005, and their vital statuses as of April 2009 were ascertained. Hospital records were examined to determine the cause of any deaths. When contact with patients was lost, we contacted them or their families by telephone. All deaths were classified into the following five groups: (1) respiratory diseases other than lung cancer, (2) lung cancer, (3) cardiac diseases, (4) malignancy other than lung cancer, and (5) other. Although the primary outcome was respiratory mortality, we also evaluated mortality from respiratory diseases (respiratory failure and lung cancer) and cardiac diseases as well as mortality from all causes because deaths from cardiac diseases are common in patients with COPD.[18] The respiratory diseases examined included respiratory failure and lung cancer. The study exclusion criteria were as follows: a smoking history < 20 pack-years, comorbidity involving respiratory disorders other than COPD, history of lung operation, aged < 40 years, and the presence of long-term oxygen therapy. This study was approved by the Ethics Committee of Kyoto University (E-772), and all subjects or their families gave oral or written informed consent.

Pulmonary Function Tests and CT Scan Acquisition

Pulmonary function tests (PFTs), subdivisions of lung volume, spirometry, and DLCO using the single-breath method were measured with a Chestac-65V (Chest MI Corp.; Tokyo, Japan). Arterial blood gas analysis also was performed in 152 subjects. Predicted PFT values were obtained from the Japanese Respiratory Society guidelines.[19]

At study entry, three thin-sectioned CT scans (upper, middle, and lower lung fields) were obtained for determination of low attenuation areas (LAA) from all 251 subjects. The same scanner (X-Vigor; Toshiba; Tokyo, Japan) and protocol were used with the following technical parameters: 2-mm thickness, 120 kVp, 200 mA, 320-mm field of view, lung reconstruction algorithm, and no contrast media. During the scan, the subjects laid in a supine position and held their breath after a deep inspiration. The PFTs usually were performed on the same day as CT scanning or within 3 months before or after CT scanning.

COPD Diagnosis

Most of data were taken before the publication of the Global Initiative for Chronic Obstructive Lung Disease (GOLD). Therefore, to reveal a range of COPD severity in the patients, COPD stages were reassessed in April 2009 following the GOLD publication.

Analysis of LAA

Air density sampled from the intrathoracic tracheal air of each subject was used to correct a calibration error due to the measurements of CT scan numbers caused by x-ray tube aging, which was in addition to the routine calibration of the CT scanner using air and water phantoms.[20] To quantitatively evaluate pulmonary emphysema, the percentage of the lung field occupied by LAA (LAA%) was measured automatically according to previously described methods.[20-23] Briefly, routine helical CT scans were performed on the entire lung and 10-mm-thick slices to exclude other lung diseases such as lung cancer and TB. However, the scans of the 10-mm-thick slices were not suitable for LAA evaluation; thus, only three thin-sectioned CT scans were obtained for determination of LAA. A cranial (upper) section was obtained 1 cm above the superior margin of the aortic arch, a middle section was taken at 1 cm below the carina, and a caudal (lower) section was taken approximately 3 cm above the top of the diaphragm to reduce the total radiation dose. In our previous study, we reported that these three slices were suitable for the evaluation of emphysema. Therefore, three sections were used to analyze LAA%.[24] The LAA% of the upper, middle, and lower lung fields was also measured.[22] The lung fields were defined as areas with CT scan numbers < −200 Hounsfield units (HU), and the cutoff level between the LAA and normal lung density was defined as −960 HU.[20-23,25] We used −960 HU as the cutoff level between the normal lung density area and the LAA.

Statistical Analysis

All statistical analyses were performed using JMP software (SAS Institute Inc.; Cary, NC). Univariate and multivariate Cox proportional hazards analyses were performed to investigate the relationship between clinical indices and mortality. Because continuous risk factor variables have no obvious clinical cutoff point for defining healthy vs unhealthy groups, they were divided into two groups according to the method of Martinez et al.[17] Namely, the poorest performing quintile (20%) became the least-healthy group, and the remaining 80% became reference groups. Data are expressed as mean ± SD. A $P < .05$ was considered to be significant.

Results

Baseline Characteristics

Table 1 shows the subjects' baseline characteristics. The number of patients with COPD in each GOLD stage[1] was as follows: stage I, 14; stage II, 111; stage III, 90; and stage IV, 36. Because of poor lung function, three subjects did not bear the diffusion capacity test.

Table 1—*Baseline Characteristics (n = 251)*

Characteristic	Value	Range
Age, y	68.7 ± 7.0	47-88
Sex		
Male	236	...
Female	15	...
BMI, kg/m^2	21.4 ± 3.0	14.0-29.5
Smoking history		
Current-smoker	97	...
Former-smoker	154	...
Smoking index, pack-y	62.8 ± 31.8	20.0-240.0
FEV_1, L	1.35 ± 0.52	0.32-2.97
FEV_1, % predicted	50.3 ± 17.0	10.0-95.1
RV/TLC, %	47.0 ± 10.1	26.1-78.0
DLCO/VA, mL/min/mm Hg/L	3.18 ± 1.21	0.70-7.94
DLCO/VA, % predicted	72.1 ± 27.1	16.8-186.0
LAA%	22.1 ± 11.8	2.3-53.9

Data are presented as mean ± SD or counts. DLCO = diffusing capacity of the lung for carbon monoxide; LAA% = the percentage of the lung field occupied by low attenuation areas; RV/TLC = residual volume/total lung capacity; VA = alveolar volume.

Prognostic Research

The median follow-up time as of April 2009 was 2,933 days (range, 215-5,107 days). At the time of analysis, it was not possible to ascertain the vital statuses of 10 of the 251 subjects because they had moved away and could not be contacted (follow-up rate, 96%). Thus, their mortality data were censored as of the date of their last visit to Kyoto University Hospital. Seventy-nine of the remaining subjects died. The causes of death were as follows: respiratory diseases (n = 40), lung cancer (n = 13), cardiac diseases (n = 5), malignancy other than lung cancer (n = 3), and other (n = 18).

Cox Proportional Hazards Analyses

The relationships among mortality from respiratory diseases other than lung cancer, mortality from respiratory and cardiac diseases, mortality from all causes, and clinical indices were analyzed with univariate Cox proportional hazards analyses (Table 2). Older age (hazard ratio [HR], 1.65; 95% CI, 1.16-2.28; $P = .0062$), higher LAA% (HR, 1.86; 95% CI, 1.35-2.55; $P = .0002$), lower BMI (HR, 1.70; 95% CI, 1.22-2.33; $P = .0025$), lower percent-predicted FEV_1 (HR, 1.51; 95% CI, 1.09-2.06; $P = .0142$), higher residual volume/total lung capacity (RV/TLC) (HR, 1.84; 95% CI, 1.33-2.51; $P = .0003$), and lower DLCO/alveolar volume (VA) (HR, 1.95; 95% CI, 1.34-2.75; $P = .0007$) were significantly related to mortality from respiratory diseases. The same indices were significant for mortality from respiratory and cardiac diseases. Percent-predicted FEV_1 was not the predictive value for mortality from all causes. In 152 of the 251 subjects who underwent arterial blood gas analysis, partial oxygen pressure was not a risk factor for mortality ($P = .4792$).

As in a previous report from Martinez et al,[17] we evaluated the relationship between mortality and LAA% in the upper lung field and lower lung field separately. Both upper lung field LAA% (HR, 2.06; 95% CI, 1.50-2.81; $P < .0001$) and lower lung field LAA% (HR, 1.55; 95% CI, 1.10-2.14; $P = .015$) were significantly correlated with mortality. However, the difference in percent emphysema (upper lung-lower lung) was not associated with mortality in the present study.

After performing multivariate Cox proportional hazards analysis using age, LAA%, BMI, FEV_1, RV/TLC, and DLCO/VA, only age and LAA% were found to be predictors of mortality from respiratory diseases (Table 3). For mortality from respiratory and cardiac diseases and mortality from all causes, BMI, age, and LAA% were predictive values (Table 3). Both analyses revealed that LAA% predicts COPD mortality independent of respiratory function. When we analyzed the data after eliminating the 10 censored subjects, we obtained similar results (data not shown). Figure 1 shows Kaplan-Meier survival curves of the LAA% subgroups.

Discussion

This study demonstrated that emphysema as assessed by CT imaging is a good predictor of mortality in patients with COPD with various stages of the disease. We documented that increased mortality was independently associated with increased age, higher LAA%, lower BMI, lower FEV_1, higher RV/TLC, and lower DLCO/VA. Multivariate analyses indicated that a higher LAA% was associated with mortality independently of increased age, lower BMI, lower FEV_1, and lower DLCO/VA. Thus, the extent of emphysema may have stronger associations with mortality in patients with COPD than other physiologic parameters.

A similar finding was previously reported in patients with AATD.[16,26] Consequently, LAA% appears to be a good predictor of mortality in patients with COPD and with and without AATD. However, Martinez et al[17] reported that the overall percentage of emphysema as assessed by CT scan was not associated with increased mortality in patients with COPD without AATD in the National Emphysema Treatment Trial (NETT). Nevertheless, their study showed that the distribution of emphysema was predictive of mortality, with improved survival seen in patients with greater emphysema in the upper lung field than in the lower lung field. Although we also examined the difference in LAA% between the upper and lower lung fields, it was not correlated with mortality in the

Table 2—*Univariate Mortality Model for All Deaths in 251 Patients With COPD*

Variable	No.	HR (95% CI) Respiratory	*P* Value	HR (95% CI) Respiratory + Cardiac Diseases	*P* Value	HR (95% CI) All	*P* Value
Age							
74.6-88.8 y	51	1.65 (1.16-2.28)	.006	1.72 (1.29-2.25)	< .0001	1.72 (1.34-2.17)	< .0001
47.9-74.5 y	200	Reference		Reference		Reference	
Smoking index							
84.0-240.0 pack-y	50	1.32 (0.88-1.89)	.163	1.24 (0.88-1.69)	.199	1.18 (0.87-1.54)	.274
20.0-82.5 pack-y	201	Reference		Reference		Reference	
BMI							
14.01-18.75 kg/m^2	51	1.70 (1.22-2.33)	.003	1.63 (1.24-2.12)	< .001	1.51 (1.18-1.90)	< .001
18.81-29.48 kg/m^2	200	Reference		Reference		Reference	
FEV_1							
0.32-0.88 L	50	1.66 (1.20-2.26)	.003	1.36 (1.02-1.77)	.035	1.25 (0.97-1.58)	.083
0.90-2.97 L	201	Reference		Reference		Reference	
FEV_1 % predicted							
10.0%-34.6%	50	1.51 (1.09-2.06)	.014	1.32 (0.99-1.71)	.056	1.23 (0.96-1.55)	.099
34.7%-95.1%	201	Reference		Reference		Reference	
RV/TLC							
55.9%-78.0%	51	1.84 (1.33-2.51)	< .001	1.66 (1.27-2.16)	< .001	1.53 (1.21-1.93)	< .001
26.1%-55.8%	200	Reference		Reference		Reference	
DLCO/VA							
0.70-2.12 mmol/min/kPa/L	50	1.95 (1.34-2.75)	< .001	1.77 (1.30-2.37)	< .001	1.52 (1.14-2.17)	< .005
2.13-7.94 mmol/min/kPa/L	198	Reference		Reference		Reference	
LAA%							
32.4%-53.9%	51	1.86 (1.35-2.55)	< .001	1.77 (1.35-2.29)	< .0001	1.52 (1.20-1.91)	< .001
2.3%-32.3%	200	Reference		Reference		Reference	
u-LAA%							
41.62%-77.81%	51	2.06 (1.50-2.81)	< .001	1.81 (1.39-2.34)	< .0001	1.55 (1.22-1.95)	< .001
1.40%-41.19%	200	Reference		Reference		Reference	
l-LAA%							
31.12%-60.25%	51	1.55 (1.10-2.14)	.015	1.60 (1.21-2.08)	.002	1.41 (1.09-1.78)	.009
2.00%-30.76%	200	Reference		Reference		Reference	
Difference in % emphysema (upper-lower)							
−30.94-−6.53	51	0.69 (0.41-1.06)	.096	0.79 (0.53-1.09)	.161	0.85 (0.62-1.12)	.263
−6.17-65.47	200	Reference		Reference		Reference	

HR = hazard ratio; l-LAA% = LAA% in the lower lung; u-LAA% = LAA% in the upper lung. See Table 1 for expansion of other abbreviations.

present study. We speculate that this discrepancy may have been caused by several factors. First, disease severity was different between studies. Centrilobular emphysema generally is most prominent in the upper lung field early in disease and becomes more diffuse as its severity increases. The subjects in our study population presented with various stages of COPD (GOLD stages I- IV), whereas subjects in the NETT had at least moderately severe disease, which might limit the study potential. The difference in the pattern of LAA% distribution may have influenced this result.

Second, our median follow-up time of 8 years was longer than that of the NETT (3.9 years). Third, the

Table 3—*Significant Predictors in Multivariate Mortality Models for All Deaths in 251 Patients With COPD*

Variable	No.	HR (95% CI) Respiratory	*P* Value	HR (95% CI) Respiratory + Cardiac Diseases	*P* Value	HR (95% CI) All	*P* Value
Age							
74.6-88.8 y	51	1.89 (1.25-2.78)	< .01	1.87 (1.35-2.55)	< .001	1.81 (1.38-2.34)	< .0001
47.9-74.5 y	200	Reference		Reference		Reference	
BMI							
14.01-18.75 kg/m^2	50	1.34 (0.93-1.91)	.112	1.36 (1.00-1.81)	.048	1.30 (1.00-1.87)	.049
18.81-29.48 kg/m^2	201	Reference		Reference		Reference	
LAA%							
32.4%-53.9%	51	1.74 (1.18-2.54)	< .01	1.65 (1.20-2.25)	.002	1.45 (1.10-1.90)	.009
2.3%-32.3%	200	Reference		Reference		Reference	

See Tables 1 and 2 for expansion of abbreviations.

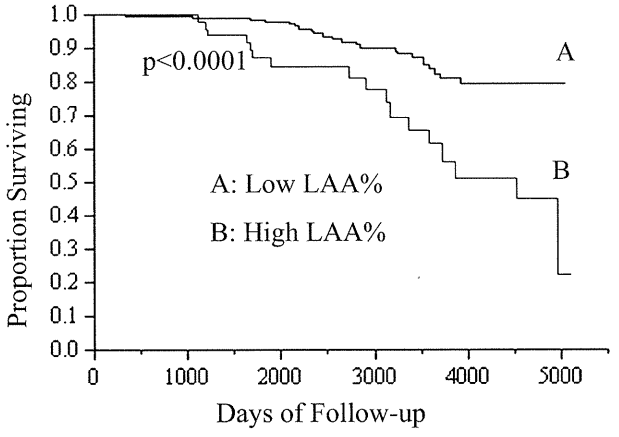

FIGURE 1. Kaplan-Meier survival curve for patients with COPD stratified by LAA%. The patients with a high LAA% showed a poor prognosis compared with those with a low LAA%. LAA% = the percentage of the lung field occupied by low attenuation areas.

NETT was a multicenter study, whereas we performed CT scans and PFTs in a single hospital with the same equipment, allowing us to avoid the inconsistencies introduced by interscanner variability.[27] We also evaluated patients with various stages of disease using a unified method that we believe to be reliable.

Several studies have indicated that patients with emphysema show more continuous inflammation than those without emphysema. Boschetto et al[28] reported a positive correlation between the high-resolution CT score for emphysema and the sputum neutrophil count, whereas Damiano et al[29] showed that the tissue neutrophil elastase distribution was related to the severity of pathologic emphysema. Furthermore, the progression of emphysema seen on CT scans was found to be associated with the initial markers of neutrophil migration.[30] Thus, chronic continuous inflammation may contribute to disease deterioration and increased mortality.

It is now generally recognized that COPD is associated with systemic manifestations, such as skeletal muscle wasting, cachexia, osteoporosis, pulmonary hypertension, ischemic heart disease, and depression.[31,32] In support of this recognition, we previously showed that BMI and loss of bone mineral density correlate with the extent of emphysema.[15,33] Although it is still unclear whether emphysema predisposes patients with COPD to such systemic manifestations and whether systemic manifestations contribute to the development of emphysema, it is apparent that the extent of emphysema is important in evaluating the COPD condition. Taken together, the evaluation of emphysema seems to be beneficial for the management of COPD. The present study shows the importance of *in vivo* evaluation of the extent of emphysema using CT imaging.

Our study has some other limitations. First, the study population did not receive uniform treatment, such as the use of inhaled corticosteroids, inhaled bronchodilators, and other drugs; therefore, it was impossible to demonstrate the influence of treatment. Second, the retrospective nature of this study prevented us from evaluating dyspnea, health status, and exercise capacity because these indices were established as risk factors for COPD mortality after we had started CT data collection.[4] Third, we did not consider the influence of comorbidities, which have been reported to play an important role in the prediction of survival in patients with COPD.[34] For these reasons, our findings may not be applicable to all patients with COPD, and larger scale studies that adjust for disease severity are needed to investigate the effects of therapeutic factors.

CONCLUSIONS

In conclusion, the extent of emphysema, as assessed by CT scan, is a good predictor of mortality in patients with COPD. This study suggests that CT imaging is a useful tool not only for detecting emphysema but also for predicting mortality in patients with COPD.

ACKNOWLEDGMENTS

Author contributions: *Dr Haruna:* contributed to the protocol design, data collection, analysis, and writing of the manuscript.
Dr Muro: contributed to the protocol design, data collection, analysis, and editing of the manuscript.
Dr Nakano: contributed to the data collection, analysis, and review of the manuscript.
Dr Ohara: contributed to the protocol design and editing of the manuscript.
Dr Hoshino: contributed to the data collection.
Dr Ogawa: contributed to the data collection.
Dr Hirai: contributed to the protocol design.
Dr Niimi: contributed to the protocol design.
Dr Nishimura: contributed to the data collection and review of the manuscript.
Dr Chin: contributed to the protocol design.
Dr Mishima: contributed to the data analysis and supervised the study.
Financial/nonfinancial disclosures: The authors have reported to *CHEST* that no potential conflicts of interest exist with any companies/organizations whose products or services may be discussed in this article.

REFERENCES

1. Rabe KF, Hurd S, Anzueto A, et al; Global Initiative for Chronic Obstructive Lung Disease. Global strategy for the diagnosis, management, and prevention of chronic obstructive pulmonary disease: GOLD executive summary. *Am J Respir Crit Care Med.* 2007;176(6):532-555.
2. Anthonisen NR, Wright EC, Hodgkin JE. Prognosis in chronic obstructive pulmonary disease. *Am Rev Respir Dis.* 1986;133(1):14-20.
3. Hansen EF, Phanareth K, Laursen LC, Kok-Jensen A, Dirksen A. Reversible and irreversible airflow obstruction as predictor